

# Continuum corrections to the level density and its dependence on excitation energy, $n$ - $p$ asymmetry, and deformation.

R. J. Charity and L. G. Sobotka

*Department of Chemistry, Washington University, St. Louis, Missouri 63130.*

In the independent-particle model, the nuclear level density is determined from the neutron and proton single-particle level densities. The single-particle level density for the positive-energy continuum levels is important at high excitation energies for stable nuclei and at all excitation energies for nuclei near the drip lines. This single-particle level density is subdivided into compound-nucleus and gas components. Two methods were considered for this subdivision. First in the subtraction method, the single-particle level density is determined from the scattering phase shifts. In the Gamov method, only the narrow Gamov states or resonances are included. The level densities calculated with these two methods are similar, both can be approximated by the backshifted Fermi-gas expression with level-density parameters that are dependent on  $A$ , but with very little dependence on the neutron or proton richness of the nucleus. However, a small decrease in the level-density parameter was predicted for some nuclei very close to the drip lines. The largest difference between the calculations using the two methods was the deformation dependence on the level density. The Gamov method predicts a very strong peaking of the level density at sphericity for high excitation energies. This leads to a suppression of deformed configurations and, consequently, the fission rate predicted by the statistical model is reduced in the Gamov method.

PACS numbers: 21.10.Ma,24.60.Dr,25.70.Jj

Keywords: level density

## I. INTRODUCTION

The nuclear level density  $\rho$  is an essential ingredient in calculating the statistical decay of a compound nucleus (CN) by particle evaporation, gamma-ray emission, or fission. The statistical model has widespread use in nuclear physics and applied research. All told in these areas, knowledge of the level density is needed at low and high excitation energies, with small and large compound-nucleus spins, and for the full range of  $Z$  and  $N$  from around the  $\beta$  line of stability out towards the drip lines. For example, the cross sections for neutron capture on nuclei close to the neutron and proton drip lines are of interest in  $r$  and  $rp$  nucleosynthesis calculations. If the excitation energy in these reactions is sufficient, the statistical model is used to determine the  $n$  and  $\gamma$  decay rates of the fused system. In such applications, level densities are required for nuclei with extreme  $n$ - $p$  asymmetries. For many of these nuclei, it will not be possible to measure the level density even with proposed radioactive beam facilities. Clearly a good understanding of the dependence of the level density on the  $n$ - $p$  asymmetry is required to extrapolate to these systems. Even for less exotic compound nuclei closer to the  $\beta$  line of stability, an asymmetry dependence can have important consequences on the  $n$ - $p$  asymmetry of the evaporation residues[1]. For fission decay, the deformation dependence of the level density is also needed. Therefore it is important to know the excitation-energy, asymmetry, and deformation dependencies of the level density over most regions of the chart of nuclides.

A complete understanding of the nuclear level density requires consideration of the many-body nature of the nucleus. However, the independent-particle model provides

a useful reference to start with. It also permits a rapid survey of level-density dependencies over many regions of the chart of nuclides and gives insight into how different nuclear-structure effects modify the level density. Many-body effects such as the effective-nucleon masses and collective enhancement due to rotational and vibrational collective modes can be incorporated in a phenomenological way onto the independent-particle model[2, 3]. In this paper, the excitation-energy,  $n$ - $p$  asymmetry, and deformation dependencies of the level density are investigated within the framework of the independent-particle model. Specifically, the role of the continuum of positive-energy single-particle states is studied. For systems around the  $\beta$  line of stability these states are populated significantly only at large excitation energies. However for systems closer to the drip lines, where either the neutron or proton separation energy is small, these states can be populated significantly even at low excitation energies. It has been suggested that the contributions from these continuum states may lead to a  $n$ - $p$  asymmetry dependence of level density[4]. The manner in which these states influence the deformation and excitation-energy dependencies of the level density will also be investigated.

Before further discussion of the level density, it is useful to first consider the largest excitation energies for which it is meaningful to apply the statistical model. The CN is a system of nucleons which is equilibrated in its single-particle degrees of freedom and thus has a long lifetime compared to the timescale of single-particle motion. As such, compound-nucleus decay is a rare process, i.e., the typically energy fluctuation of a nucleon, which is of order of the temperature  $T$ , does not lead to the emission of that particle. Thus, the regime of applicability is  $T < E_{cost}^{\min}$  where  $E_{cost}^{\min}$  is the minimum of  $E_{cost}^n$  and  $E_{cost}^p$ ,

the energetic costs of emitting a neutron or a proton, respectively. For neutrons, the cost is just the neutron separation energy  $E_{cost}^n = E_{sep}^n$ , while for protons the cost also includes the Coulomb barrier  $E_{cost}^p = E_{sep}^p + V_{coul}$ .

The decay width for protons or neutrons is roughly[5]

$$\Gamma = \frac{t^2}{\pi\epsilon_0} \exp(-E_{cost}/t) \quad (1)$$

where  $\epsilon_0 = \hbar^2/2mR^2$ ,  $1/t = d\rho/dE^*$  is the nuclear temperature ( $t \approx T$ ),  $m$  is the nucleon mass, and  $R$  is the nuclear radius. As  $t$  approaches  $E_{cost}^{\min}$ , the decay width for either proton or neutron evaporation becomes quite large. For the statistical model to be applicable, the total decay width must be small compared to the spreading width which determines the time scale for the CN to equilibrate.

The order of this paper is as follows. A brief review of the level density in the independent-particle model is given in Sec. II. Subsequently, two methods to include the positive-energy states are considered in Sec. III. Following this in Sec. IV, the details of the coupled-channels calculation of the single-particle level densities are given. The determination of the deformation energy is discussed in Sec. VI and calculated level densities are presented in Sec. VII. Finally in Secs. VIII and IX, a discussion of the results and the conclusions of this work are made.

## II. LEVEL DENSITY IN THE INDEPENDENT-PARTICLE MODEL

The independent-particle model starts with sets of single-particle levels for both neutrons and protons. The determination of the nuclear level density is essentially a combinatorial problem, i.e., how many ways can these single-particle levels be occupied to give the desired total excitation energy. However, the enumeration of all the single-particle configurations can be avoided. Instead, the Laplace transform  $Z(\alpha, \beta)$  of the level density is more easily calculated when the Lagrange multipliers  $\alpha$  and  $\beta$  are introduced to constraint the total number of particles and the total energy. The inverse transform can be obtained from the saddle-point approximation to give a formula for the level density which is continuous in excitation energy  $E^*$ . For simplicity at this point, consider only one type of nucleon with single-particle levels  $\epsilon_i$ , the level density is then[6]

$$\rho(E^*) = \frac{\exp S}{2\pi\sqrt{D}} \quad (2)$$

where  $S = \beta E - \alpha A + \ln Z(\alpha, \beta)$ . The values of the Lagrange multipliers are determined by the saddle-point condition  $\partial S/\partial\beta = \partial S/\partial\alpha = 0$ . Now the average occupancy of a single-particle level is given by  $f_i = 1/[1 + \exp(\beta\epsilon_i - \alpha)]$ . Thus the saddle-point condition can be expressed in terms of the conservation of nucleon

number  $A$  and total energy  $E = E_{gs} + E^*$  (ground-state + excitation energy) by

$$A = \frac{\partial \ln Z}{\partial \alpha} = \sum_i f_i, \quad (3)$$

$$E = E_{gs} + E^* = -\frac{\partial \ln Z}{\partial \beta} = \sum_i \epsilon_i f_i. \quad (4)$$

At the saddle point, the quantities  $Z$ ,  $D$ , and  $S$  are now

$$\ln Z = \sum_i \ln [1 + \exp(\alpha - \beta\epsilon_i)], \quad (5)$$

$$D = \begin{vmatrix} \frac{\partial^2 \ln Z}{\partial \alpha^2} & \frac{\partial^2 \ln Z}{\partial \alpha \partial \beta} \\ \frac{\partial^2 \ln Z}{\partial \beta \partial \alpha} & \frac{\partial^2 \ln Z}{\partial \beta^2} \end{vmatrix}, \quad (6)$$

and

$$S = \sum_i s_i. \quad (7)$$

Here

$$s_i = -f_i \ln f_i - (1 - f_i) \ln (1 - f_i). \quad (8)$$

Although this formula can be derived without recourse to statistical mechanics, Bethe[7] realized there is a close analogy to the problem of a Fermi gas in contact with a heat bath of temperature  $T=1/\beta$  and with chemical potential  $\mu=\alpha/\beta$ . In this analogy,  $Z$  is the grand partition function,  $S$  is the entropy and thus  $1/T = dS/dE^*$ .

If the single-particle level-density  $g(\epsilon) = \sum_i \delta(\epsilon - \epsilon_i)$  is constant (at least in the vicinity of  $\epsilon=\mu$ ), then Eq. 2 can be reduced to the well known Bethe or Fermi-gas expression[6, 7, 8]:

$$\rho(E^*) = \frac{\exp S}{\sqrt{48E^*}}, \quad (9)$$

$$S = 2\sqrt{aE^*} = aT^2, \quad (10)$$

where  $a = \frac{\pi^2}{6} g(\mu)$  is the level-density parameter. For a two-component Fermi gas, the level density parameter will have contributions from each component  $a = \frac{\pi^2}{6} [g_n(\mu_n) + g_p(\mu_p)]$ . Experimentally, level-density parameters exhibit strong shell corrections at low excitation energies. However apart from this, the average value of the level-density parameter is often assumed to depend only linearly on  $A$  with no dependence on the  $n$ - $p$  asymmetry.

To gauge the temperatures for which this formula should be applied, the functions  $f$  (Fermi function) and  $s$ , which are needed to determine the total energy and entropy (Eqs. 4 and 7), are plotted in Fig. 1 versus  $\beta\epsilon - \alpha = (\epsilon - \mu)/T$ . The Fermi function  $f$ , giving the average level occupancy, changes in value from 90% to 10% over an interval  $\Delta\epsilon = 4.4T$  centered around  $\mu$ . The function  $s$  is Gaussian-like with a full width half maximum (FWHM) of  $4.2T$ , however the tails of the function falls off much slower than a Gaussian. The Fermi-gas

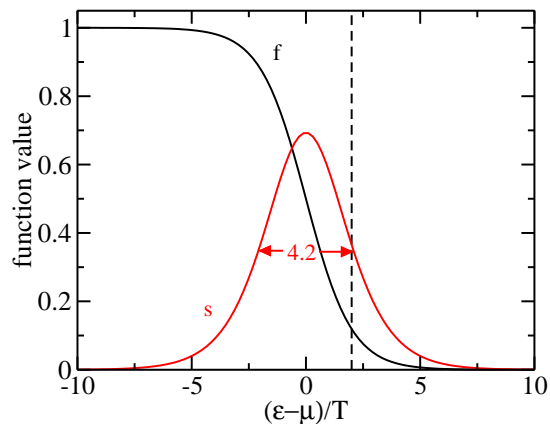


FIG. 1: (Color online) The evolution with  $(\varepsilon - \mu)/T$  of the functions  $f$  and  $s$  (Eq. 8) used to determine the total energy and entropy. The vertical dashed line indicates the location of the  $\varepsilon=0$ , when  $T=E_{sep}/2$ .

formula thus assumes the single-particle level density  $g$  is constant at least over an interval  $\pm 2T$  around  $\mu$ . However because  $s$  falls off so slowly, the contribution to the entropy from levels at smaller and larger energies are not insignificant. Therefore at large temperatures, how useful is the Fermi-gas formula when  $g$  is not constant? At low temperatures by expanding Eqs. 3, 4, and 7 as functions of  $T$ , the entropy with its lowest-order correction becomes  $S = \sqrt{a'E^*}$  where

$$a' = a \left[ 1 + \frac{7g(\mu_0)g''(\mu_0) - 5g'(\mu_0)^2}{5g(\mu_0)^3} E^* \right], \quad (11)$$

$\mu_0$  is the chemical potential at  $T=0$ , and  $g'$  and  $g''$  are the first and second derivatives of  $g$ . Thus the level-density parameter can be replaced by an effective level-density parameter  $a'$  which is excitation-energy dependent. Higher-order corrections will be needed at larger temperatures.

What about the role of positive energy states? Consider a system where  $T = E_{sep}/2$ . In Fig. 1 for this case,  $\varepsilon=0$  would correspond to the vertical dashed line and clearly, because  $s$  decreases so slowly with  $\varepsilon$ , the positive-energy states (those beyond the dash line) are important for the entropy.

### III. CONTINUUM SINGLE-PARTICLE LEVEL DENSITY

In order to understand the role of positive-energy states in calculating the level density, we need a prescription for deciding which of these positive-energy levels belong to the CN. If there is no bounding volume enclosing the nucleus, the single-particle level density of these states is infinite. However not all of these states are considered to be associated with the CN. To better understand the selection of positive-energy states belonging

to the CN, one can consider the problem of nucleon evaporation. This is often dealt with by placing the CN in a box whose volume is large compared to the nuclear volume. Call this state  $i$ . The box volume  $V$  can eventually be expanded and allowed to approach infinity. If the CN decays by the emission of a nucleon with kinetic energy  $\varepsilon$  to state  $f$ , then as we have a bounding box, the nucleon cannot escape and will eventually be reabsorbed by the daughter nucleus leading us back to state  $i$ . Therefore by the general principle of detailed balance, the transition probability  $P_{if}$  from state  $i$  to  $f$  is related to that of the inverse process by

$$\rho_i P_{if} = \rho_f P_{fi} \quad (12)$$

where  $\rho_i$  and  $\rho_f$  are the density of states for  $i$  and  $f$ , respectively. For state  $i$ , the density of states is just the level density of the compound nucleus  $\rho_i = \rho_{CN}(E^*)$ . While for state  $f$ , both the level density of the daughter nucleus  $\rho_d$  and the phase space  $g_{ev}$  of the evaporated particle contribute, i.e.,

$$\rho_f = \rho_d(E^* - E_{sep} - \varepsilon) g_{ev}(\varepsilon) d\varepsilon. \quad (13)$$

Now

$$\begin{aligned} g_{ev}(\varepsilon) &= (2s + 1) \frac{4\pi p^2}{h^3} V \frac{dp}{d\varepsilon} \\ &= (2s + 1) \frac{(2m)^{3/2} V \sqrt{\varepsilon}}{4\pi^2 h^3} \end{aligned} \quad (14)$$

where  $p$ ,  $m$  and  $s$  are the evaporated nucleon's momentum, mass and spin, respectively. Here  $g_{ev}$  is determined for an empty box in the semiclassical limit. This should be appropriate as the box volume is large. Because  $P_{fi} = v \sigma_{inv}(\varepsilon)/V$ , then

$$\begin{aligned} P_{if} &= \frac{\Gamma(\varepsilon) d\varepsilon}{h} \\ &= \frac{(2s + 1)m}{(\pi\hbar)^2} \varepsilon \sigma_{inv}(\varepsilon) \frac{\rho_d(E^* - E_{sep} - \varepsilon)}{\rho_{CN}(E^*)} d\varepsilon \end{aligned} \quad (15)$$

where  $v$  is the nucleon velocity and  $\sigma_{inv}$  is the inverse or absorption cross section.

In this derivation of the Weisskopf evaporation formula, the single-particle level density contributes to both  $\rho_{CN}$  and the phase space of the evaporated nucleon  $g_{ev}$ . Thus for a given nuclear mean-field potential surrounded by a bounding box, the total single-particle level density will be subdivided;  $g_{tot}(\varepsilon) = g_{CN}(\varepsilon) + g_{gas}(\varepsilon)$  where  $g_{CN}$  is the single-particle level density used to calculate the compound-nucleus level density and the remaining level density  $g_{gas}$  is associated with a gas of evaporated particles. Thus  $g_{gas} \sim g_{ev}$ , where  $g_{ev}$  is the single-particle level density for the empty bounding box, i.e., without the nuclear mean-field potential (Eq. 14). As the box volume is chosen to be much larger than the nuclear volume, then we also find  $g_{tot} \sim g_{ev}$ , though of

course  $g_{tot} \neq g_{gas}$ . With such a subdivision of  $g_{tot}$ , the nucleon number in the box can be subdivided, i.e.,

$$\begin{aligned} A_{tot} &= \int g_{tot}(\varepsilon) d\varepsilon = \int g_{CN}(\varepsilon) d\varepsilon + \int g_{gas}(\varepsilon) d\varepsilon \\ &= A_{CN} + A_{gas}. \end{aligned} \quad (16)$$

Similarly  $E_{tot} = E_{CN} + E_{gas}$  and  $S_{tot} = S_{CN} + S_{gas}$ . For a given temperature, the chemical potential  $\mu$  is constrained so that  $A_{CN}$  is the constant value appropriate for the CN. Thus  $A_{gas}$  and  $A_{tot}$  will be temperature dependent and hence  $1/T = dS_{CN}/dE_{CN}$  while  $dS_{tot}/dE_{tot} \neq 1/T \neq dS_{gas}/dE_{gas}$ .

The quantity  $g_{CN}$  should contain all the negative-energy bound states located in the well of the nuclear-plus-Coulomb potential. For positive energies,  $g_{CN}$  should be independent of the bounding volume. However apart from these constraints, there is no well justified subdivision of  $g_{tot}$  into its two components in the independent-particle model. Two methods have been utilized to calculate  $g_{CN}$ .

### A. Subtraction Method

In 1978 Fowler, Engelbrecht, and Woosley[9] proposed that  $g_{gas} \equiv g_{ev}$  for neutrons and thus  $g_{CN}$  could be obtained from subtraction, i.e.,  $g_{CN} = g_{tot} - g_{ev}$ . We will call this the subtraction method for determining  $g_{CN}$  and it has been used by many other investigators. It is rather easy to show that[10, 11, 12, 13]

$$g_{CN}^{sub}(\varepsilon) = \sum_{\ell,j} g_{\ell,j}(\varepsilon), \quad (17)$$

$$\begin{aligned} g_{\ell,j}(\varepsilon) &= (2j+1) \sum_i \delta(\varepsilon - \varepsilon_i^{\ell,j}) \\ &\quad + \frac{1}{\pi} (2j+1) \frac{d\delta_{\ell,j}}{d\varepsilon} \end{aligned} \quad (18)$$

where  $\delta_{\ell,j}(\varepsilon)$  is the phase shift associated with the scattering state of energy  $\varepsilon$ , orbital angular momentum  $\ell$ , and total angular momentum  $j$ . The bound-state energies are  $\varepsilon_i^{\ell,j}$ . From Levinson's theorem[11],

$$\int_{-\infty}^{\infty} g_{\ell,j}(\varepsilon) d\varepsilon = 0. \quad (19)$$

It is clear that for  $\varepsilon > 0$ ,  $g_{\ell,j}$  must have a net negative contribution to balance out the positive contributions from the bound states. However, for the large  $\ell$  waves, this negative contribution occurs at very large  $\varepsilon$  values which are not populated in the CN[12]. Thus the negative contributions are only important for the lowest  $\ell$ -waves.

Near a resonance

$$\frac{d\delta_{\ell,j}}{d\varepsilon} = \frac{\Gamma^R/2}{(\varepsilon - \varepsilon^R)^2 + (\Gamma^R/2)^2} \quad (20)$$

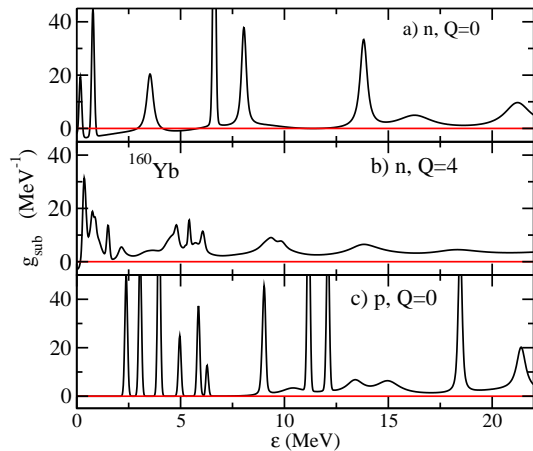


FIG. 2: (Color online) The dependence of the compound-nucleus single-particle level density  $g_{CN}^{sub}$  on the nucleon energy  $\varepsilon$ . The displayed results have been convoluted by a Gaussian resolution of FWHM=150 keV. Results are shown for a) neutron in a spherically symmetric potential ( $Q=0$ ), b) neutrons in a deformed potential ( $Q=4$ ), and c) protons in a spherically symmetric potential.

where  $\varepsilon^R$  is the resonance energy and  $\Gamma^R$  is its width. In the limit as  $\Gamma^R \rightarrow 0$ ,  $d\delta_{\ell,j}/d\varepsilon \rightarrow \pi \delta(\varepsilon - \varepsilon^R)$  and the resonance becomes equivalent to a bound state. Therefore at positive energies,  $g_{CN}^{sub}$  consists of series of resonance peaks which, for low  $\ell$ -waves, sit on a negative background.

For protons, the single-particle level density is calculated from the nuclear phase shift, not the total phase shift. Hence, the subtracted level density is not actually  $g_{ev}$ , the contribution from the bounding volume without any mean-field potential, as used for neutrons. In this case, the subtracted level density is that from the bounding volume containing a point-source Coulomb potential. For deformed systems, the  $\varepsilon > 0$  contribution can be generalized as[14, 15, 16]

$$g_{CN}^{sub}(\varepsilon) = \frac{1}{2\pi i} \text{Tr} \left( \mathbf{S}^{-1}(\varepsilon) \frac{d}{d\varepsilon} \mathbf{S}(\varepsilon) \right) \quad (21)$$

where  $\mathbf{S}(\varepsilon)$  is the S-matrix for scattering at energy  $\varepsilon$ .

Examples of  $g_{CN}^{sub}(\varepsilon)$  calculated for  $^{160}\text{Yb}$  are shown in Fig. 2. The negative background is clearly observable in Fig. 2a for neutrons in a spherically-symmetric potential. Here  $g_{CN}^{sub}(\varepsilon)$  is negative between the resonance peaks for  $\varepsilon < 6$  MeV. In deforming the potential, degenerate resonances are split and this often leads to a filling up of the negative background so that  $g_{CN}^{sub}$  seldom drops below zero. For the deformed example in Fig. 2b,  $g_{CN}^{sub}$  is only negative at  $\varepsilon \sim 0$ . For protons (Fig. 2c), only very narrow resonances are observed well below the Coulomb barrier ( $\varepsilon \sim 9$  MeV).

## B. Gamov Method

By placing the CN in a bounding box, we have produced an equilibrium model. Now within this equilibrium model, any arbitrary subdivision of  $g_{tot}$  into  $g_{CN}$  and  $g_{gas}$  can be considered. Whatever subdivision is made, the inverse cross section  $\sigma_{inv}$  must be chosen to describe the absorption of nucleons from the “gas” phase space into the “compound-nucleus” phase space. However, in order for the equilibrium evaporation rate to be equated to that of an isolated CN which is a nonequilibrium problem,  $g_{CN}$  should be chosen such that  $f(\varepsilon)g_{CN}(\varepsilon)$  also describes the nucleon energy-density when there is no gas present. As  $g_{CN}^{sub}$  can be negative for some energies, the number of nucleons ascribed to the CN in these single-particle levels is also negative. In the equilibrium model, this does not pose a problem as we have an accompanying gas in the box. The total number of nucleons in any energy range is always positive, i.e.,  $g_{tot} > 0$ . It is just our prescription of dividing up  $g_{tot}$  into  $g_{CN}$  and  $g_{gas}$  that gives rise to this problem. However in the absence of the gas, it is not clear what physical significance a negative value of  $g_{CN}$  has.

Another criticism of the subtraction method is that it includes both narrow (long-lived) and wide (short-lived) resonances. It has been suggested that only resonances of lifetime longer than, or comparable to, the compound-nucleus lifetime should be included[17, 18] as the occupancy of the shorter-lived levels will not be maintained before the CN decays.

Consider the analytical continuation of the S-matrix into the complex-energy plane. Poles of the S-matrix at  $\varepsilon = \varepsilon^R - i\Gamma^R/2$  correspond to exponentially decaying solutions to the Schrödinger equation (if  $\Gamma^R > 0$ )[13, 19]. These are also known as Gamov[20] or Siegert states. For those poles close to the real axis on the unphysical sheet, these states have a close association with resonances. Weidenmüller[17] suggested the compound-nucleus single-particle level density for  $\varepsilon > 0$  should be the density of sharp resonances or Gamov states. One should therefore introduce a cutoff or maximum width  $\Gamma_0$  of the Gamov states that contribute to  $g_{CN}$ . Now, if the single-particle potential is modified, for example by deformation, the location of the poles will move in the complex-energy plane. Some will become narrower and some wider and a number of these will cross the cutoff region causing discontinuities in the level density as it evolves with deformation. In order to avoid such discontinuities, a smooth exponential cutoff of the Gamov states was implemented;

$$g_{CN}^\Gamma(\varepsilon) = \sum_i \delta(\varepsilon - \varepsilon_i^R) \exp\left(\frac{-\Gamma_i^R}{\Gamma_0}\right). \quad (22)$$

The summation includes all poles associated with bound states ( $\Gamma^R=0$ ) and Gamov states ( $\Gamma^R > 0$ ). With this definition,  $g_{CN}^\Gamma$  is always positive and thus avoids the ambiguities associated with negative values as in  $g_{CN}^{sub}$ . In the

following sections, both definitions of  $g_{CN}$  will be used to see how they affect the excitation-energy, deformation, and asymmetry dependencies of the level density.

## IV. COUPLED-CHANNELS CALCULATION OF SINGLE-PARTICLE LEVELS

### A. Theory

In order to calculate the single-particle level densities, the Schrödinger equation must be solved to determine the bound, Gamov, and scattering states. Protons and neutrons are assumed to move in an axially-symmetric mean-field potential which is the sum of the nuclear, Coulomb, and spin-orbit components, i.e.,

$$V(\mathbf{r}) = V_N(\mathbf{r}) + V_C(\mathbf{r}) + V_{so}(\mathbf{r}). \quad (23)$$

The nuclear potential is expressed in terms of the Fermi function  $f(x) = [1 + \exp(x)]^{-1}$  as

$$V_N(\mathbf{r}) = -V_N^{(0)} f\left(\frac{r - R(Q, \theta)}{d(\theta)}\right) \quad (24)$$

where  $R(Q, \theta)$  defines a spheroidal surface with the same volume as a sphere of radius  $R^{(0)}$ . The deformation is expressed in terms of the relative quadrupole moment  $Q$  related to the radii,  $r_{\parallel}$  and  $r_{\perp}$ , perpendicular and parallel to the symmetry axis by [21]

$$Q = \frac{8\pi}{15} \frac{(r_{\parallel}^2 - r_{\perp}^2)}{[R^{(0)}]^2}. \quad (25)$$

The quadrupole moment is positive for prolate shapes, negative for oblate, and zero at sphericity. As a calibration point,  $Q=3.2$  corresponds to a “superdeformed” prolate shape with the length of the major and minor axes differing by a factor of 2.

The diffuseness of the nuclear potential is assumed to be constant perpendicular to this surface, i.e.,

$$d(\theta) = d^{(0)} \sqrt{1 + \left(\frac{dR}{d\theta} \frac{1}{R}\right)^2}. \quad (26)$$

The deformed spin-orbit interaction can be expressed in terms of the momentum  $\mathbf{p}$  and spin  $\mathbf{s}$  operators as[22]

$$V_{so}(\mathbf{r}) = 4V_{so}^{(0)} \left( \left[ \nabla f\left(\frac{r - R_{so}(Q, \theta)}{d_{so}(\theta)}\right) \right] \times \mathbf{p} \right) \cdot \mathbf{s} \quad (27)$$

where  $d_{so}$  is defined in terms of  $R_{so}$  in an equivalent manner as in Eq. 26. The Coulomb potential is approximated as that from a sharp-surfaced spheroid of equivalent spherical radius  $R_C$  using the analytical expressions of Refs. [23, 24]. The parameters  $V_N^{(0)}$ ,  $V_{so}^{(0)}$ ,  $R^{(0)}$ ,  $R_{so}^{(0)}$ ,  $R_C$ , and  $d^{(0)}$  are taken from the “universal” parametrization of Ref. [25].

The solutions to the Schrödinger equation  $H\Psi = \varepsilon\Psi$  are obtained by expressing the wavefunction as sums of spherical waves specified by  $|\ell\frac{1}{2}jm\rangle$ . Here  $\ell$  is the orbital angular momentum,  $j$  is the total angular momentum and  $m$  is its projection on the symmetry axis. This latter quantity is conserved in the axially-symmetric potential. Thus

$$\Psi_m(\mathbf{r}) = \sum_{\ell,j} \frac{u_{\ell jm}(r)}{r} |\ell\frac{1}{2}jm\rangle \quad (28)$$

---


$$\left[ \frac{d^2}{dr^2} + k^2 - \frac{\ell(\ell+1)}{r^2} \right] u_{\ell jm}(r) + \sum_{\ell',j'} \left( W_{\ell j \ell' j'}^m(r) + D_{\ell j \ell' j'}^m(r) \frac{d}{dr} \right) u_{\ell' j' m}(r) = 0. \quad (29)$$


---

Here  $k = \sqrt{2\mu\varepsilon}/\hbar$  is the wave number and  $\mu$  is the reduced mass. The matrices  $\mathbf{W}$  and  $\mathbf{D}$  are determined from the matrix elements of the interaction taken between states specified by  $\ell, j$  and  $\ell', j'$ . The matrix  $\mathbf{W}$  has contributions from all three potentials (nuclear, Coulomb, and spin-orbit) while  $\mathbf{D}$  is determined only from the spin-orbit potential.

The boundary conditions at the origin are  $u_{\ell jm}(0)=0$ . If one considers  $N$  channels and chooses  $N$  initial sets of the derivatives  $du_{\ell jm}/dr(0)$  appropriately, then after integrating out from the origin, one can obtain  $N$  independent solutions to the coupled-channels equation. Let these be represented by the  $N$  columns of the  $N \times N$  matrix  $\mathbf{U}^m(r)$ . In matrix form, the Schrödinger equation is then

$$\left[ \frac{d^2}{dr^2} + \mathbf{D}^m(r) \frac{d}{dr} + \mathbf{A}^m(r) \right] \mathbf{U}^m(r) = 0 \quad (30)$$

where

$$A_{\ell j \ell' j'}^m = \left[ k^2 - \frac{\ell(\ell+1)}{r^2} \right] \delta_{\ell\ell'} \delta_{jj'} + W_{\ell j \ell' j'}^m. \quad (31)$$

The equation is integrated out to a radius  $r_{\text{match}}$  where  $V \rightarrow 0$  for neutrons or, for protons, only a point-source Coulomb term is present. At  $r_{\text{match}}$ , the solutions are matched to specific solutions of the Schrödinger equations  $p_\ell(r)$ . For bound states, the matching solution must vanish as  $r \rightarrow \infty$  and thus  $p_\ell(r) = \sqrt{2|k|r/\pi} K_{\ell+\frac{1}{2}}(|k|r)$  or  $p_\ell(r) = W_{-\eta, \ell+\frac{1}{2}}(2|k|r)$  for neutrons and protons, respectively. Here  $K_{\ell+\frac{1}{2}}$  are the modified Bessel functions of the second kind and  $W_{-\eta, \ell+\frac{1}{2}}$  are the Whittaker functions and  $\eta = (Z-1)e^2/(\hbar^2|k|)$ . For Gamov states, the matching functions are outgoing waves;  $p_\ell(r) = kr [j_\ell(kr) + i y_\ell(kr)]$  or  $p_\ell(r) = F_\ell(\eta, kr) - i G_\ell(\eta, kr)$  for neutrons and protons respectively. Here  $j_\ell$  and  $y_\ell$  are the regular and irregular spherical Bessel functions and  $F_\ell$  and  $G_\ell$  are regular and irregular Coulomb wavefunctions. If the calculated solution is to

where  $u_{\ell jm}(r)$  are the radial wavefunctions. After projecting on the state  $|\ell'\frac{1}{2}j'm\rangle$ , the Schrödinger equation can be written in terms of the coupled-channels equation

represent a bound or Gamov state, then one must be able match the logarithmic derivatives of  $u_{\ell jm}$  and  $p_\ell$  at  $r = r_{\text{match}}$  for all channels. Any linear combination of the column vectors of  $\mathbf{U}^m$  can be used to achieve this match and it is only possible when[26]

$$\left| \frac{d\mathbf{U}^m}{dr} (\mathbf{U}^m)^{-1} - \frac{d\mathbf{P}}{dr} (\mathbf{P})^{-1} \right|_{r=r_{\text{match}}} = 0 \quad (32)$$

where the matrix  $\mathbf{P}$  is defined as

$$P_{\ell j \ell' j'}(r) = \delta_{\ell\ell'} \delta_{jj'} p_\ell(r). \quad (33)$$

The matrix  $\mathbf{Y} = d\mathbf{U}^m/dr (\mathbf{U}^m)^{-1}$  is called the log-derivative matrix and satisfies the following Riccati equation

$$\frac{d\mathbf{Y}}{dr} + \mathbf{A} + \mathbf{Y}^2 + \mathbf{D}\mathbf{Y} = 0. \quad (34)$$

Rather than solving the matrix Schrödinger equation (Eq. 30), this equation can be solved directly using the techniques of Refs. [27, 28, 29]. In fact, it is advantageous to solve the Riccati equation instead of the Schrödinger equation as the latter suffers from numerical instabilities when integrating over classically forbidden regions.

To obtain scattering solutions, the wavefunctions must be matched to a combination of ingoing and outgoing waves at  $r = r_{\text{match}}$ . The scattering matrix can also be obtained directly from the log-derivative[27]. Defining the matrix elements

$$\begin{aligned} J_{\ell j \ell' j'}(r) &= \delta_{\ell\ell'} \delta_{jj'} kr j_\ell(kr) \text{ for neutrons} \\ &= \delta_{\ell\ell'} \delta_{jj'} F_\ell(kr) \text{ for protons} \end{aligned} \quad (35)$$

$$\begin{aligned} N_{\ell j \ell' j'}(r) &= \delta_{\ell\ell'} \delta_{jj'} kr y_\ell(kr) \text{ for neutrons} \\ &= -\delta_{\ell\ell'} \delta_{jj'} G_\ell(kr) \text{ for protons,} \end{aligned} \quad (36)$$

the  $\mathbf{K}$  matrix is determined by

$$\begin{aligned} \mathbf{K} &= - \left[ \mathbf{Y}(r_{\text{match}}) \mathbf{N}(r_{\text{match}}) - \frac{d}{dr} \mathbf{N}(r_{\text{match}}) \right]^{-1} \\ &\quad \times \left[ \mathbf{Y}(r_{\text{match}}) \mathbf{J}(r_{\text{match}}) - \frac{d}{dr} \mathbf{J}(r_{\text{match}}) \right]. \end{aligned} \quad (37)$$

The  $S$  matrix is derived in terms of the identity matrix  $I$  as

$$S = (I + iK)^{-1} (I - iK). \quad (38)$$

The calculation of  $g_{CN}^{sub}$  from Eq. 21 can be problematic near very narrow resonances. However, the level density convoluted with a small dispersion is more easily determined. If  $F(\varepsilon)$  is the convolution function, the convoluted level density is

$$\tilde{g}_c(\varepsilon) = \int_0^\infty g_c(\varepsilon') F(\varepsilon - \varepsilon') d\varepsilon'. \quad (39)$$

Following Sandulescu *et al.*[30], the integral along the real axis can be replaced by a contour integral in the complex-energy plane which avoids narrow resonances. The contour  $C$  is chosen to follow the real axis except near resonances with  $\Gamma < 50$  keV where it follows a semi-circular path of radius 0.2 MeV around each resonance. From Cauchy's theorem, the final level density is

$$\tilde{g}_c(\varepsilon) = \sum_n F(\varepsilon - \varepsilon_n^R) + \int_C g_c(\varepsilon') F(\varepsilon - \varepsilon') d\varepsilon' \quad (40)$$

where here  $\varepsilon_n = \varepsilon_n^R - i\Gamma_n^R/2$  is the complex energy of the  $n$ th avoided resonance. The convolution function  $F$  was taken as Gaussian with FWHM=150 MeV. This small resolution does not have any significant affect on the deduced level densities in this work.

## B. Results

An example of the evolution of bound single-particle levels and the real part of narrow Gamov states ( $\Gamma < 0.5$  MeV) with deformation is shown in Fig. 3 for  $m^\pi = \frac{1}{2}^-$  neutrons in  $^{190}\text{Yb}$ . The results were obtained by including all channels with  $\ell \leq 20$  in the coupled-channels calculations. The bound states and resonances levels both move around with deformation, but levels of the same  $m^\pi$  values avoid crossing each other. Bound levels that pass through  $\varepsilon=0$  immediately become narrow resonances and vice versa. As the resonance energy increases, the width of a resonance generally increases as shown in Fig. 3.

The behavior that bound states turn into narrow resonances is quite general except if there is no barrier (centrifugal or Coulomb)[13]. For  $j = \frac{1}{2}^+$  ( $\ell=0$ ) neutrons there is no barrier and bound states passing through  $\varepsilon=0$  turn into virtual states[13]. A virtual state is associated with a pole of the S matrix on the real  $\varepsilon$  axis at energy  $\varepsilon_v = -e_v$  ( $e_v > 0$  and small). Both bound and virtual states have real negative energies and purely imaginary wavenumbers  $k$ . However for bound states, the imaginary part of  $k$  is positive while it is negative for virtual states. In fact when there is no barrier, both bound and virtual states with small energies have important influences on the scattering at small positive values of  $\varepsilon$ . This has implications

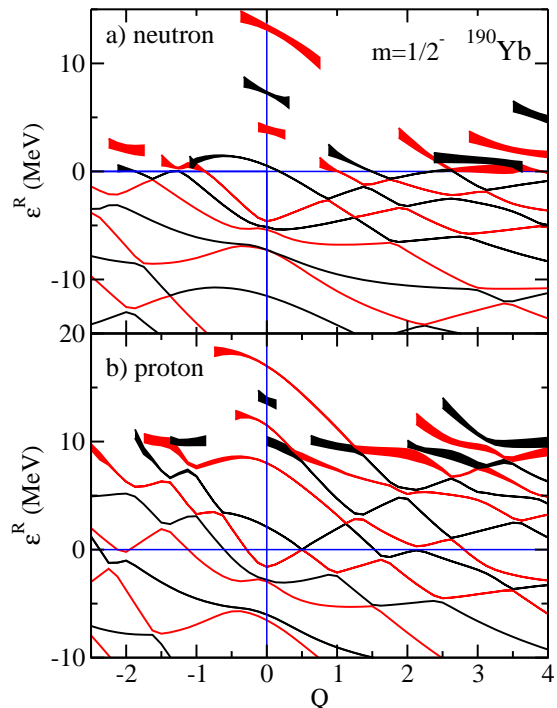


FIG. 3: (Color online) Evolution of the real energy  $\varepsilon^R$  for bound ( $\varepsilon^R < 0$ ,  $\Gamma^R=0$ ) and narrow Gamov ( $\varepsilon^R > 0$ ,  $\Gamma^R < 1$  MeV) states as a function of deformation. The width of the curves reflects the value of  $\Gamma^R$ . Results are only shown for a) neutron and b) proton  $m^\pi = \frac{1}{2}^-$  states in  $^{190}\text{Yb}$ .

for the single-particle level density calculated with the subtraction method. Consider a spherically symmetric potential. The  $\ell=0$  contribution to the single-particle level density from a virtual state for small  $\varepsilon$  values is[13]

$$g_0^{sub}(\varepsilon) = \begin{cases} \frac{1}{2\pi} \sqrt{\frac{e_v}{\varepsilon}} \frac{1}{\varepsilon + e_v} & \text{if } \varepsilon > 0, \\ 0 & \text{if } \varepsilon < 0. \end{cases} \quad (41)$$

On the other hand for a bound state at  $\varepsilon_b = -e_b$  ( $e_b > 0$  and small), the contribution is[13]

$$g_0^{sub}(\varepsilon) = \begin{cases} -\frac{1}{2\pi} \sqrt{\frac{e_b}{\varepsilon}} \frac{1}{\varepsilon + e_b} & \text{if } \varepsilon > 0 \\ = \delta(\varepsilon + e_b) & \text{if } \varepsilon < 0. \end{cases} \quad (42)$$

As  $\varepsilon \rightarrow +0$ ,  $g_0^{sub} \rightarrow +\infty$  for the virtual state and  $-\infty$  for the bound state. In the limit that  $e_v \rightarrow 0$  and  $e_b \rightarrow 0$ , then in both cases  $g_0^{sub}(\varepsilon) \rightarrow \delta(\varepsilon)/2$  and this represents half a level. Thus in the deformation region over which a bound level becomes a virtual state,  $g_{CN}^{sub}$  evolves smoothly.

Only the  $m = \frac{1}{2}^+$  states contain any  $j = \frac{1}{2}^+$  ( $\ell=0$ ) component in their wavefunction. For these states, the behavior as a bound state passes through  $\varepsilon=0$  is more complex. Sometimes they become narrow resonances, sometimes they become virtual states, and other times they

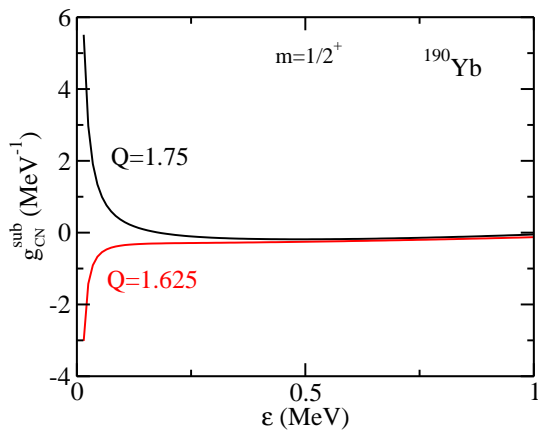


FIG. 4: (Color online) Variation with nucleon energy  $\varepsilon$  of the single-particle level density determined by the subtraction method for  $m^\pi=1/2^+$  neutrons in  $^{190}\text{Yb}$ . Results are shown for two neighboring deformations  $Q=1.75$  and  $1.625$ .

progress in complicated manner to a wider resonance. As an example, Figure 4 shows the  $m=\frac{1}{2}^+$  contribution to the single particle level-density  $g_{1/2^+}^{\text{sub}}(\varepsilon)$  at small positive energies obtained for two neighboring values of  $Q$ . For  $Q=1.625$ ,  $g_{1/2^+}^{\text{sub}} \rightarrow -\infty$  as  $\varepsilon \rightarrow +0$  as in Eq. 42. On the other hand, at  $Q=1.75$ ,  $g_{1/2^+}^{\text{sub}} \rightarrow +\infty$  as in Eq. 41. In this case the behavior of  $g_{1/2^+}^{\text{sub}}$  is consistent with a bound state at  $Q=1.625$  passing through  $\varepsilon=0$  and becoming a virtual state at  $Q=1.75$ .

For the Gamov method,  $g_{1/2^+}^\Gamma(\varepsilon)$  does not evolve smoothly when a bound state becomes a virtual state; bound states are always counted as a full level while virtual states are not counted at all in Eq. 22. However, virtual states can cause long time delays in scattering like narrow resonances[19] and some thought should be given to expanding the definition of  $g_{CN}^\Gamma$  to include some contribution from virtual states and so make the evolution with  $Q$  smoother. In the present work this is not a significant issue as, in the range of deformation investigated ( $-2.5 < Q < 4$ ), there is typically only 2 small discontinuities.

To visualize the gross differences between the subtraction and Gamov methods it is useful to smooth the single-particle level density  $g_{CN}$ . Figure 5 displays smoothed neutron and proton single-particle level densities  $\widetilde{g}_{CN}$  for  $^{160}\text{Yb}$ . The Strutinsky smoothing discussed in Sec. VI was utilized. For neutrons,  $\widetilde{g}_{CN}$  peaks near  $\varepsilon=0$ . The peak is lower in magnitude for the subtraction method due to the presence of the negative background. As resonances at larger  $\varepsilon^R$  tend to have larger widths, the Gamov method, which excludes these wide resonances, makes  $\widetilde{g}_{CN}$  drop quickly to zero for  $\varepsilon \gg 0$ . The effect is more pronounced the smaller the cutoff width  $\Gamma_0$ . Protons exhibit similar behavior except they peak closer to the Coulomb barrier whose magnitude is indicated by the arrow in Fig. 5b.

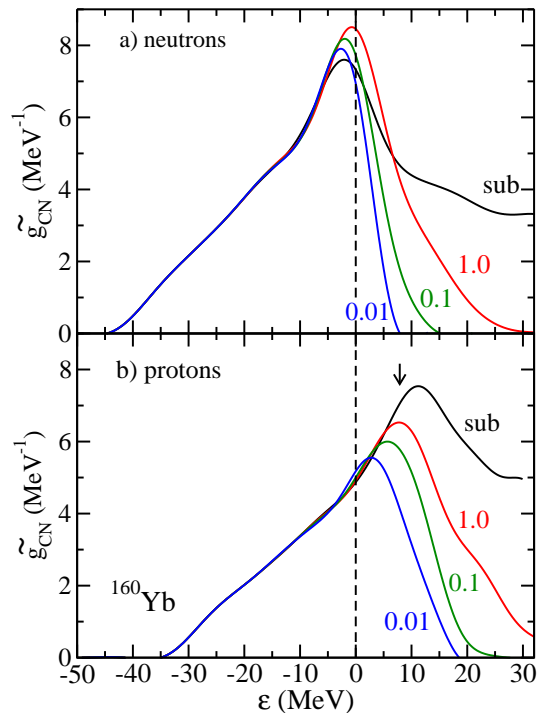


FIG. 5: (Color online) Smoothed single-particle level densities calculated for a) neutrons and b) protons in  $^{160}\text{Yb}$ . The curves labeled “sub” were obtained from the subtraction method. The other curves were obtained from the Gamov method with the indicated values of  $\Gamma_0$  in MeV. The Coulomb barrier for protons is indicated by the arrow in b).

There are two important results to highlight. First for protons,  $g(\varepsilon)$  is almost independent of the method of calculation for small positive energies well below the Coulomb barrier. These positive-energy states have the most influence of the level density and thus the continuum corrections for protons will generally be less important than those for neutrons. Secondly for neutrons, the inclusion of the negative background and the wide resonances in the subtraction method have opposite effects and partially cancel. In the end, the level densities calculated with both methods are found to be similar (see Sec. VII A).

The subtraction method does not give a strong deformation dependence of  $\widetilde{g}_{CN}$  near sphericity. As an example, the smoothed single-particle level density for neutrons in  $^{160}\text{Yb}$  is plotted in Fig. 6a for  $Q=-0.5, 0, 0.5$ . The curves for all three deformations lie almost on top of each other. In contrast, the Gamov method exhibits a strong dependence. The results, displayed in Fig. 6b for  $\Gamma_0=1$  MeV, show that  $\widetilde{g}_{CN}$  decreases in magnitude for  $\varepsilon > 0$  as a deformation is imposed on the compound nucleus (either prolate or oblate). To investigate this behavior, let us concentrate on the splitting of Gamov states which are degenerate at sphericity. For example in Fig. 7, the evolution with deformation of the energy and width for a group of Gamov states associated with

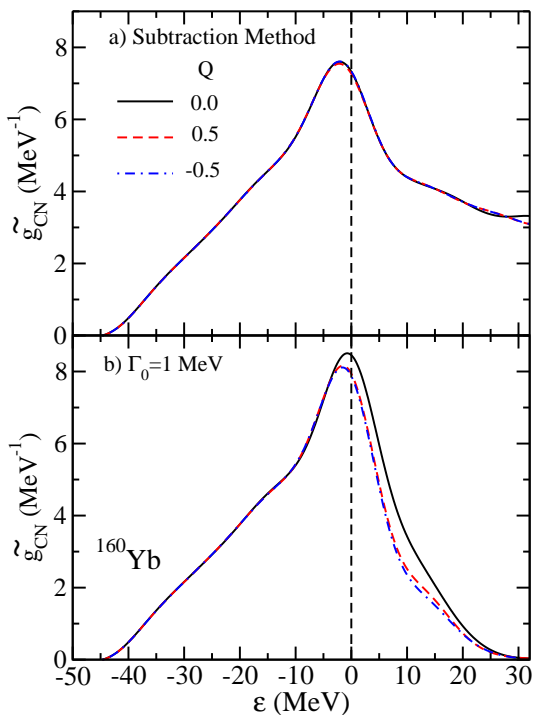


FIG. 6: (Color online) Smoothed single-particle level densities calculated for neutrons in  $^{160}\text{Yb}$  at three deformations;  $Q = -0.5, 0$ , and  $0.5$ . In a) results obtained with the subtraction method are displayed while in b), the Gamov method with  $\Gamma_0 = 1$  MeV was used.

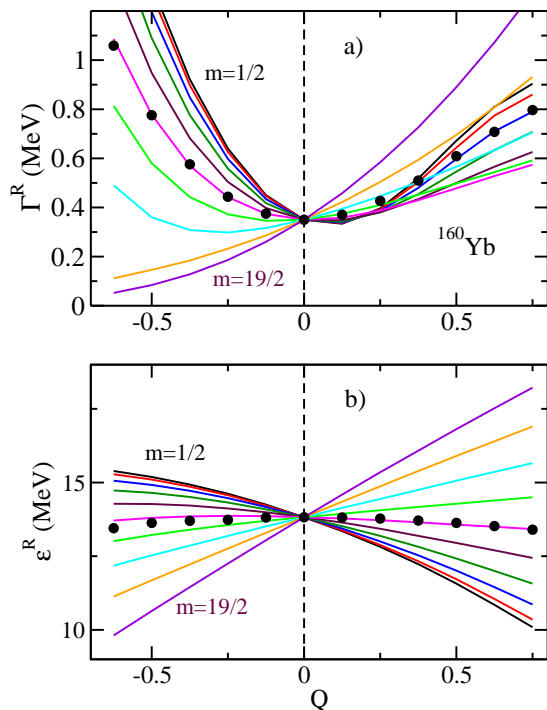


FIG. 7: (Color online) Curves show the variation with deformation  $Q$  of the energy  $\epsilon^R$  and width  $\Gamma^R$  of the Gamov states associated with the  $j=19/2^-$  neutrons in  $^{160}\text{Yb}$ . The solid data points indicate the average energy and width for these states.

$j=19/2^-$  neutrons in  $^{160}\text{Yb}$  is displayed. In Fig. 7b, the real energies  $\epsilon^R$  of the Gamov states fanout with increasing deformation (both oblate and prolate). On average, the mean value of  $\epsilon^R$  changes very little with deformation. These mean values are indicated by the data points. In contrast, the widths  $\Gamma^R$  of Gamov states show a different behavior in Fig. 7b. Although a few of the states for oblate deformations show a reduced width compared to sphericity, by in large the widths of most states increase with deformation. The average widths, indicated by the data points, have a minimum at sphericity. This behavior is typical of the splitting of all degenerate Gamov states and therefore the average increase in these widths with deformation reduces their contribution to  $g_{CN}^\Gamma$  (Eq. 22). This explains the observed deformation dependence displayed in Fig. 6b. The strong dependence of  $g_{CN}^\Gamma$  on deformation is reflected in the deformation dependence of the level density (see Sec. VI).

## V. NUCLEAR LEVEL DENSITY WITH PAIRING

The simple discussion of the level density in Sec. II for a single particle type and no interactions is extended in this section to include both neutrons and protons and the pairing interaction. The grand potential of a two-component Fermi gas is the sum of the proton and neutron contributions, i.e.,

$$\Omega(\alpha_n, \alpha_p, \beta) = \Omega_n(\alpha_n, \beta) + \Omega_p(\alpha_p, \beta). \quad (43)$$

The pairing interaction is considered in the BCS model[31, 32, 33]. In this model, the grand potential is related to the grand partition function ( $\Omega_n(\alpha_n, \beta) = -\ln Z_n/\beta$ ) and for neutrons it is given by

$$\begin{aligned} \Omega_n(\alpha_n, \beta) &= \frac{\Delta_n^2}{G_n} + \int \frac{g_n(\epsilon)}{2} [\epsilon - \mu_n - E] d\epsilon \\ &- \frac{2}{\beta} \int \frac{g_n(\epsilon)}{2} \ln [1 + \exp(-\beta E)] d\epsilon \end{aligned} \quad (44)$$

where  $\beta = 1/T$ ,  $T$  is the temperature, and  $\mu_n = \alpha_n/\beta$  is the chemical potential. The quasiparticle energies are

$$E = \sqrt{(\epsilon - \mu_n)^2 + \Delta_n^2}. \quad (45)$$

The gap parameter  $\Delta_n$  is determined from the gap equation

$$\frac{2}{G_n} = \int \frac{g_n(\epsilon)}{2} \frac{\tanh\left(\frac{E}{2T}\right)}{E} d\epsilon \quad (46)$$

where  $G_n$  is the pairing strength. The level density at an energy  $E^{tot}$  can be obtained from the inverse Laplace transform of the grand partition function

$$\rho(E^{tot}, N, Z) = \frac{1}{(2\pi i)^3} \int_{-i\infty}^{+i\infty} \int_{-i\infty}^{+i\infty} \int_{-i\infty}^{+i\infty} Z \exp(-\alpha_n N - \alpha_p Z + \beta E) d\alpha_n d\alpha_p d\beta \quad (47)$$

which can be evaluated approximately by the saddle-point method to give

$$\rho(E^{tot}, N, Z) = \frac{\exp(S)}{(2\pi)^{3/2} \sqrt{D}}. \quad (48)$$

Here the energy ( $E^{tot} = E_n^{tot} + E_p^{tot}$ ), entropy ( $S = S_n + S_p$ ), and particle number are determined from the following equations:

$$E_n^{tot} = \int \varepsilon \frac{g_n(\varepsilon)}{2} \left[ 1 - \frac{\varepsilon - \mu_n}{E} \tanh\left(\frac{E}{2T}\right) \right] d\varepsilon - \frac{\Delta_n^2}{G_n}, \quad (49)$$

$$S_n = \int g_n(\varepsilon) \ln \left[ 1 + \exp\left(-\frac{E}{T}\right) \right] d\varepsilon + \int g_n(\varepsilon) \frac{\frac{E}{T}}{1 + \exp\left(\frac{E}{T}\right)} d\varepsilon, \quad (50)$$

$$N = \int \frac{g_n(\varepsilon)}{2} \left[ 1 - \frac{\varepsilon - \mu_n}{E} \tanh\left(\frac{E}{2T}\right) \right] d\varepsilon. \quad (51)$$

The quantities  $E_p^{tot}$ ,  $S_p$ , and  $\Delta_p$  for protons are obtained from similar expressions and the determinant  $D$  is now

$$D = \begin{vmatrix} \frac{\partial^2 \ln Z}{\partial \alpha_n^2} & \frac{\partial^2 \ln Z}{\partial \alpha_n \partial \alpha_p} & \frac{\partial^2 \ln Z}{\partial \alpha_n \partial \beta} \\ \frac{\partial^2 \ln Z}{\partial \alpha_n \partial \alpha_p} & \frac{\partial^2 \ln Z}{\partial \alpha_p^2} & \frac{\partial^2 \ln Z}{\partial \alpha_p \partial \beta} \\ \frac{\partial^2 \ln Z}{\partial \alpha_n \partial \beta} & \frac{\partial^2 \ln Z}{\partial \alpha_p \partial \beta} & \frac{\partial^2 \ln Z}{\partial \beta^2} \end{vmatrix}. \quad (52)$$

Expressions for the evaluation of this determinant in terms of the single-particle level densities can be found in Ref. [32]. At some critical temperature  $T^{crit}$ , the gap parameter vanishes and the excitation energy and entropy are those of a noninteracting Fermi gas, i.e., Eqs. 3, 4, and 7.

## VI. DEFORMATION ENERGY

The level density will be calculated as a function of excitation energy. The excitation energy is given in terms of the thermal contribution  $E_{th} = E^{tot}(T, Q) - E^{tot}(0, Q)$  and the deformation energy  $E_{def}(Q)$ . In the Strutinsky procedure[34], the deformation energy is given by two terms

$$E_{def}(Q) = \delta E(Q) + V_{def}(Q) \quad (53)$$

where the liquid-drop deformation energy  $V_{def}(Q)$  describes the average deformation energy with shell oscillations averaged out. The corrections  $\delta E(Q)$  to the liquid-drop energy are determined from the single-particle levels

and have contributions from both neutrons and protons, i.e.,  $\delta E = \delta E_n + \delta E_p$ . Following Ref. [33], we define the shell corrections as

$$\delta E_k(Q) = E_k^{tot}(0, Q) - \widetilde{E}_k^{tot}(0, Q) \quad (54)$$

where  $k=n$  or  $p$ , and  $\widetilde{E}_k^{tot}$  is the total energy determined with pairing (Eq. 49), but with the smoothed single-particle level densities

$$\widetilde{g}(\varepsilon) = \int g(\varepsilon') F(\varepsilon - \varepsilon') d\varepsilon'. \quad (55)$$

The smoothing function used is

$$F(\varepsilon) = \frac{1}{\sqrt{\pi}\gamma} \exp\left[-\left(\frac{\varepsilon}{\gamma}\right)^2\right] C_p\left(\frac{\varepsilon}{\gamma}\right) \quad (56)$$

where the smoothing range  $\gamma$  must be taken to be of the order of the intershell separation in order to washout the oscillations. The curvature correction of order  $p=2M$  is

$$C_p(x) = \sum_{n=0}^M \frac{(-1)^n}{2^{2n} n!} H_{2n}(x) = L_M^{1/2}(x^2). \quad (57)$$

This curvature correction is included to provide self-consistency for  $\widetilde{g}(\varepsilon)$ , i.e., a smoothed function should not be affected by the smoothing procedure. Thus if  $\widetilde{g}(\varepsilon)$  is a polynomial of order  $2M+1$  or lower, it will be unchanged after the smoothing. The functions  $H_n$  and  $L_p^{1/2}$  are Hermite polynomials and associated Laguerre polynomials, respectively.

In the original Strutinsky smoothing procedure, the smoothing parameters  $\gamma$  and  $p$  are chosen to satisfy the plateau condition[34, 35]

$$\frac{d\widetilde{E}_k^{tot}}{d\gamma} = 0, \quad \frac{d\widetilde{E}_k^{tot}}{dp} = 0, \quad (58)$$

over some range in both  $\gamma$  and  $p$ . Thus in this range, the shell correction should depend neither on the smoothing range or the order of the curvature correction. The plateau condition can be satisfied for single-particle levels associated with infinite potentials such as a harmonic oscillator or an infinite square well. However for a finite-depth potential, such as those considered in this work, the plateau condition is often not met, i.e., one cannot find a region of  $\gamma$  and  $p$  over which the shell correction is constant[36, 37, 38].

An alternative procedure from Refs. [37, 38] was tried, however this was found to be problematic in some cases. Instead the method that is used in this work relies on the

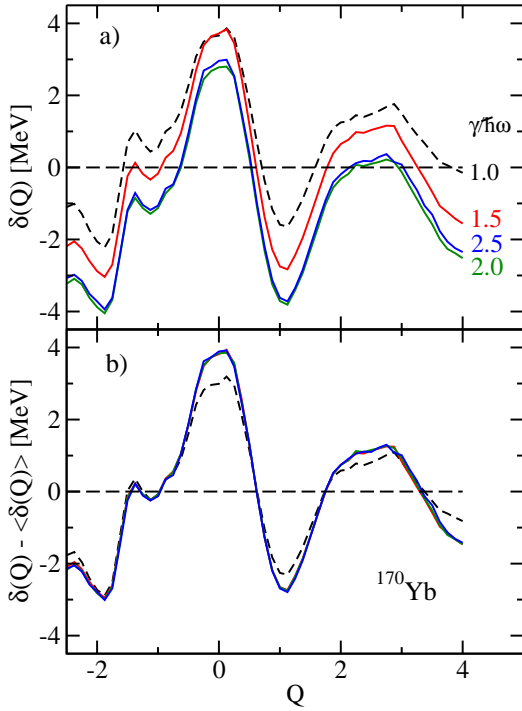


FIG. 8: (Color online) Variation of the neutron shell correction to the deformation energy determined for  $^{170}\text{Yb}$ . a) The absolute correction obtained with the indicated smoothing ranges  $\gamma$ . b) The data from a), but now the mean correction over all calculated deformations  $\langle\delta(Q)\rangle$  have been subtracted out.

observation that the relative correction for different deformations is independent of  $\gamma$  and  $p$  once  $\gamma$  has a value above  $\sim 1.2 \hbar\omega$ . The actual  $\gamma$  value at which the relative correction plateaus depends on the order  $p$  used. However once the plateau is reached, the relative corrections are independent of  $p$ . As an example, the correction factors for neutrons obtained with  $p=12$  for various  $\gamma$  values are plotted in Fig. 8a. The absolute values of these corrections vary continuously with  $\gamma$  and do not plateau. However, it does have a minimum in the interval  $2.0 < \gamma < 2.5$  in this example. Now apart from the dashed curve obtained with  $\gamma = \hbar\omega$ , all other  $\delta_n(Q)$  curves have almost the same shape indicating the relative shell correction is constant. To highlight this, the average value of the correction over all deformations  $\langle\delta_n(Q)\rangle$  is subtracted out for each smoothing range. The remaining correction  $\delta_n(Q) - \langle\delta_n(Q)\rangle$  is plotted in the Fig. 8b. All the curves for  $\gamma > \hbar\omega$  now collapse to essentially a single curve.

If we cover a large enough range of deformations, the average shell correction  $\langle\delta_k(Q)\rangle$  is expected to be zero, thus we have taken the values plotted in Fig. 8b to be absolute corrections. Thus the appropriate smoothing range is the value which causes  $\langle\delta_k(Q)\rangle = 0$ . We expect the range of deformations explored in this work ( $-2.5 < Q < 4.0$ ) to be adequate as we always see at least a couple of “oscillations” in  $\delta_k$  and thus expect the average to reflect the true average over all deformations.

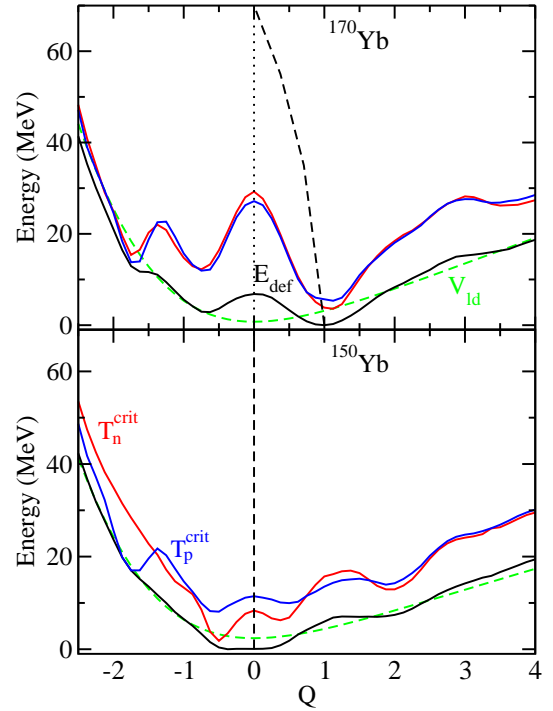


FIG. 9: (Color online) Variation of four calculated energies with deformation for  $^{170}\text{Yb}$  and  $^{150}\text{Yb}$ . The curve  $E_{def}$  is the deformation energy with shell corrections. For comparison the liquid-drop deformation energy  $V_{ld}$  is also shown. The higher two curves give the energies corresponding to the critical temperatures  $T^{crit}$  for protons and neutrons. The thick-dashed lines indicate the deformation which maximized the level density (subtraction method) for each excitation energy.

Finally the excitation energy is measured with respect to the ground-state energy, i.e., the total excitation energy is

$$E^* = E_{th} + E_{def}(Q) - \delta W. \quad (59)$$

Here the shell correction  $\delta W$  represents the difference between the liquid-drop and the minimum or ground-state deformation energy, i.e.,  $\delta W = \min[E_{def}(Q)]$ . Note that any error in the absolute value of  $\delta_k(Q)$  affects both  $E_{def}(Q)$  and  $\delta W$  equally, and therefore the excitation energy is not sensitive to the absolute shell correction.

The liquid-drop deformation energy is taken from Refs. [39, 40]. The gap strength  $G_{n,p}$  for neutrons and protons is determined from setting  $\widetilde{\Delta}_{n,p}(Q=0, T=0) = 12/\sqrt{A}$  MeV [6]. Here  $\widetilde{\Delta}_{n,p}$  is the gap parameter obtained from Eq. 46 with the smoothed single-particle level densities  $\widetilde{g}_{n,p}$ . Examples of the deformation energy are shown in Fig. 9 for systems with deformed ( $^{170}\text{Yb}$ ) and spherical ( $^{150}\text{Yb}$ ) ground states. Also shown are the excitation energies corresponding to the critical temperature  $T_{n,p}^{crit}$  for neutrons and protons where the pairing gap vanishes.

TABLE I: Nuclei studied in this work and the value of the shell correction  $\delta W$ , minimum cost  $E_{cost}^{min}$ , and pairing factor  $\delta P$ .

Nucleus	$\delta W$ (MeV)	$E_{cost}^{min}$ (MeV)	$\delta P$ (MeV)
$^{40}\text{Si}$	1.1	1.9	2.7
$^{40}\text{S}$	0.6	5.4	2.7
$^{40}\text{Ar}$	0.1	9.4	2.7
$^{40}\text{Ca}$	-0.7	7.4	2.7
$^{40}\text{Ti}$	0.6	3.1	2.6
$^{60}\text{Ti}$	-0.8	3.1	2.6
$^{60}\text{Cr}$	0.2	5.7	2.6
$^{60}\text{Fe}$	0.4	8.4	2.5
$^{60}\text{Ni}$	-0.6	10.1	2.5
$^{60}\text{Zn}$	-0.6	6.9	2.5
$^{60}\text{Ge}$	-1.6	3.8	2.6
$^{170}\text{Nd}$	0.6	2.5	2.4
$^{190}\text{Yb}$	-1.6	3.8	2.4
$^{180}\text{Yb}$	0.5	5.6	2.3
$^{170}\text{Yb}$	-0.8	7.6	2.3
$^{160}\text{Yb}$	0.7	9.9	2.2
$^{150}\text{Yb}$	-2.4	8.9	2.2
$^{170}\text{Hg}$	-2.9	10.0	2.2
$^{238}\text{U}$	-0.7	5.5	2.3

## VII. CALCULATIONS

### A. Excitation-Energy and $n$ - $p$ Asymmetry Dependencies

The level density as function of excitation energy was calculated for even-even nuclei with  $A=40$  and  $60$ . All such nuclei with  $E_{cost}^{min} > 1.9$  MeV were included in the study. These include  $^{40}\text{Ti}$  and  $^{60}\text{Ge}$  which are just beyond the proton-drip line. Calculations were also performed for five even-even Yb nuclei from  $^{150}\text{Yb}$  to  $^{190}\text{Yb}$  covering the range of  $n$ - $p$  asymmetry centered on  $\beta$ -stable nucleus  $^{170}\text{Yb}$ . In addition two other  $A=170$  nuclei,  $^{170}\text{Nd}$  and  $^{170}\text{Hg}$ , with extreme values of  $n$ - $p$  asymmetry were included. Again,  $^{150}\text{Yb}$  and  $^{170}\text{Hg}$  are just beyond the proton drip line. Finally the heavier  $\beta$ -stable system  $^{238}\text{U}$  was also studied. All nuclide studied are listed in Table I along with their values of  $\delta W$  and  $E_{cost}^{min}$ .

At each deformation  $Q$ , the level density and excitation energy are calculated for an array of temperatures each separated by  $0.05$  MeV. The level density for a given excitation energy is then obtained from interpolating between these results. Subsequently, the deformation of the nucleus at each excitation energy is determined as the value which maximizes the level density. As an example, the deformation as function of excitation energy is plotted in Fig. 9 as the thick-dashed curves. For the deformed ground-state system  $^{170}\text{Yb}$ , the deformation decreases with excitation energy and vanishes at  $E^*=70$  MeV. The spherical ground-state system  $^{150}\text{Yb}$  remains spherical at all excitation energies.

The variation of the resulting level density with exci-

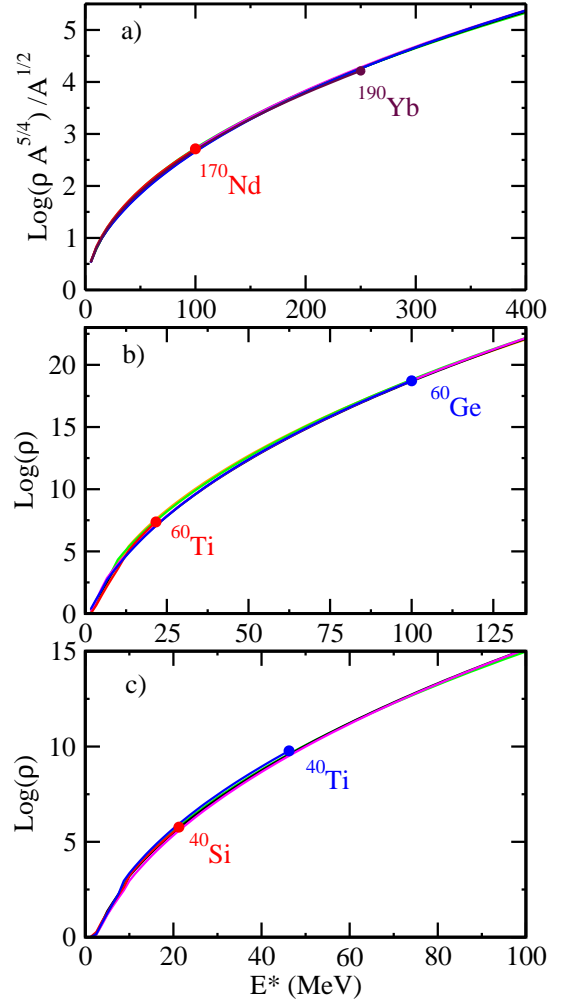


FIG. 10: (Color online) Variation of the nuclear level density with excitation energy for a) the seven  $A \sim 170$  nuclei, b) the six  $A=60$  nuclei, and c) the five  $A=40$  nuclei. All are calculated up to the excitation energy where  $T=E_{cost}^{min}$ . These values are indicated by the solid circular symbols if they are within the displayed ranges and are labelled.

tation energy obtained with the subtraction method is plotted in Figs. 10a, b, and c for  $A \sim 170$ ,  $A=60$  and  $A=40$ , respectively. In Fig. 10a where  $A$  is not constant, the quantity  $\log(\rho A^{5/4}) A^{1/2}$  rather than  $\log(\rho)$  has been plotted to account for the  $A$  dependence based on the Fermi-gas formula with  $a \propto A$ . Curves for all nuclei are only extended up to the excitation energy where  $T=E_{cost}^{min}$ . It is clear from this figure, that the level density has no substantial dependence on  $n$ - $p$  asymmetry, all curves with similar  $A$  values practically overlap. Similar conclusions were also obtained with the Gamov method. For example, the level densities for  $A \sim 170$  and  $A=40$  are shown in Figs. 11 and 12, respectively, for  $\Gamma_0=1.0$  and  $\Gamma_0=0.01$  MeV. Again, the curves for similar  $A$  values fall almost on top of each other.

For  $T > T_n^{crit}$  and  $T > T_p^{crit}$  in even-even nuclei, the excitation energy is often backshifted by the conden-

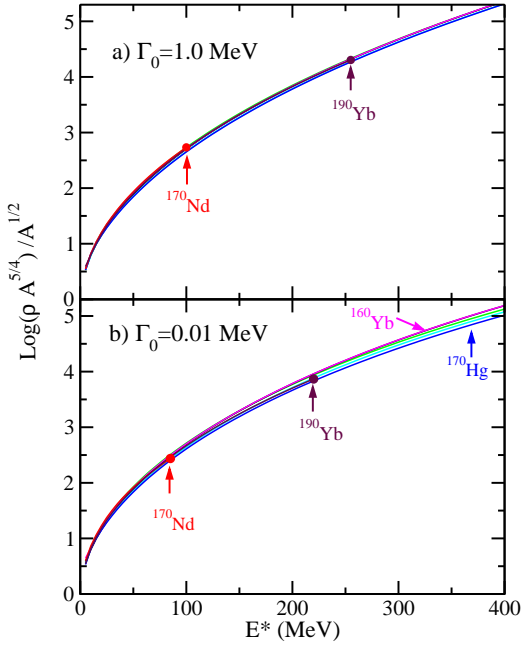


FIG. 11: (Color online) Same as for Fig. 10a, but now the level density for  $A \sim 170$  is calculated with the Gamov method using the cutoff decay widths of  $\Gamma_0=1$  and 0.01 MeV. Only curves that are distinguishable from the others are labelled.

sation energy when comparing level densities [41], i.e.,  $U=E^* - \delta P$  where the smoothed condensation energy is

$$\delta P = \frac{1}{2} \tilde{\Delta}_n^2 \tilde{g}_n(\tilde{\mu}_n) + \frac{1}{2} \tilde{\Delta}_p^2 \tilde{g}_p(\tilde{\mu}_p). \quad (60)$$

For odd-even and odd-odd nuclei,  $\delta P$  should include the pairing correction in the semiempirical mass formula. In the comparison of level densities in Figs. 10–12, the role of pairing is not important as the condensation energy is relatively constant for each mass region (see Table I). At high excitation energies where shell effects are expected to be washed out, the excitation energy is also shifted by the shell correction  $\delta W$ [42]. Thus at high energies, a shifted Fermi-gas expression is often assumed. In this case, the entropy is

$$S = 2\sqrt{\tilde{a}(E^* - \delta P + \delta W)} \quad (61)$$

where  $\tilde{a}$  is the asymptotic level-density parameter.

To see whether this formalism is consistent with the calculations of this work, the asymptotic level-density parameter is calculated from Eq. 61 for all excitation energies. Examples of the resulting level-density parameters are displayed in Fig. 13 for the subtraction method and in Figs. 14 and 15 for the Gamov method. Above  $(E^* - \delta P + \delta W)/A > 0.3$  MeV where shell and pairing effects are expected to be quenched, the deduced level-density parameter is rather constant. Note, Figs. 13–15 have offset origins on the  $y$  axis to accentuate the difference between the different nuclei. Quite surprisingly, the

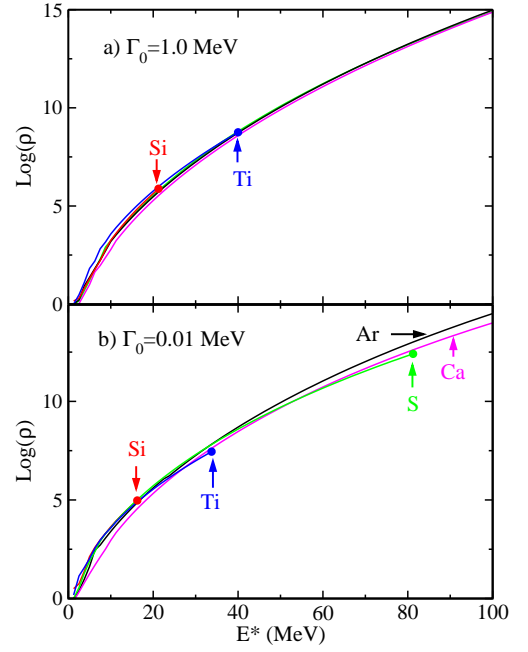


FIG. 12: (Color online) Same as for Fig. 10c, but now the level density for  $A=40$  is calculated with the Gamov method using the cutoff decay widths of  $\Gamma_0=1$  and 0.01 MeV. Only curves that are distinguishable from the others are labelled.

inclusion of realistic single-particle level densities including continuum corrections does not cause strong deviations from the basic Fermi-gas expression which was derived for constant  $g(\varepsilon)$ . A similar conclusion was found in Hartree-Fock calculations of  $^{208}\text{Pb}$  performed by Bonche, Levit, and Vautherin[43].

The dependence of  $\tilde{a}$  on excitation energy is not completely flat, all calculations show some small negative slope as is expected in a lowest-order expansion in temperature (Eq. 11). This is most significant in the Gamov method (Figs. 14b and 15b) with the smallest value of cutoff the width ( $\Gamma_0=0.01$  MeV). The plots of the asymptotic level-density parameter also highlight the small differences between the nuclei with the similar  $A$  values which were difficult to see in Figs. 10–12. The differences between the curves would become more significant if they are extended beyond the point  $T > E_{cost}^{\min}$  where the the statistical model is problematic. For  $A=40$ , the asymptotic level-density parameter can be somewhat smaller for the systems with extreme  $n$ - $p$  asymmetries. For example, look at the results for  $^{40}\text{Si}$  in Fig. 13c with the subtraction method and for  $^{40}\text{Ti}$  in Fig. 15b with  $\Gamma_0=0.01$  MeV. For both of these cases, the asymptotic region is only approach when  $E_{cost}^{\min} \approx T$ . To investigate the small  $n$ - $p$  asymmetry dependence more systematically, the value of  $\tilde{a}$  determined at  $(E^* - \delta P + \delta W)/A=0.5$  MeV is plotted in Fig. 16 as a function of  $N - N_\beta(A)$ , the distance from the  $\beta$ -valley of stability. Results are shown for the subtraction method (filled circles), and the Gamov method with three values of the maximum width;  $\Gamma_0=1$  MeV

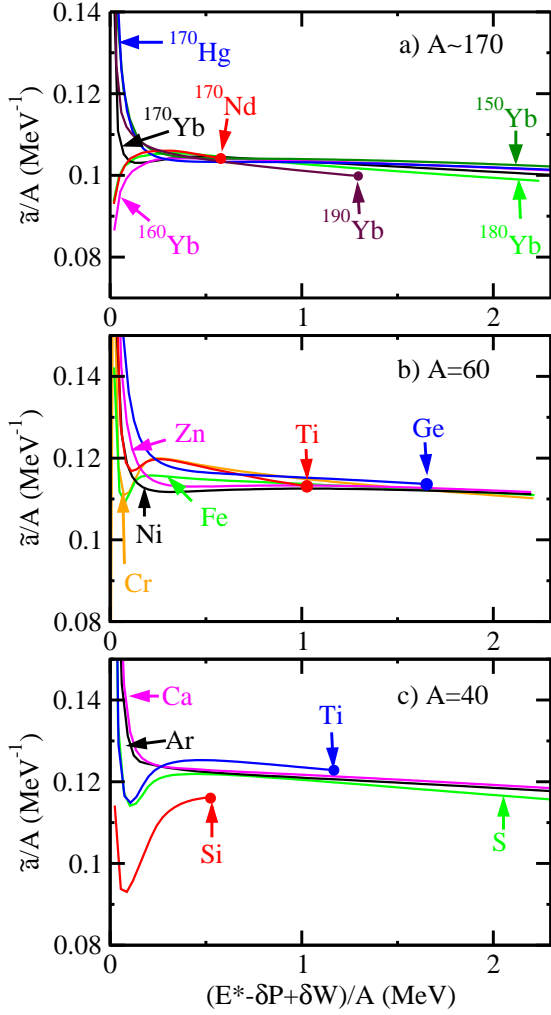


FIG. 13: (Color online) Level-density parameters  $\tilde{a}$  deduced from the calculated entropy and Eq. 61 as a function of the shifted excitation energy per nucleon. Results were obtained using the subtraction method to treat the continuum. The data points indicated on each curve are the point at which  $E_{cost}^{\min} = T$ .

(hollow squares),  $\Gamma_0 = 0.1$  MeV (filled diamonds), and  $\Gamma_0 = 0.01$  MeV (hollow triangles). Generally, the deduced values of  $\tilde{a}$  are approximately independent of which treatment of the continuum was used and are almost constant for each mass region. In the Gamov method, the nuclei with the extreme values of  $N - N_\beta(A)$  show the greatest sensitivity to  $\Gamma_0$ . In this case the values of  $\tilde{a}$  obtained with  $\Gamma_0 = 0.01$  MeV are often slightly smaller.

The mass dependence of the level-density parameter at  $(E^* - \delta P + \delta W)/A = 0.5$  MeV is displayed in Fig. 17 as the data points. The extracted points were fit by the commonly used formula

$$\tilde{a} = \alpha_v A + B_s \alpha_s A^{2/3} \quad (62)$$

which includes volume and surface contributions where  $\alpha_v$  and  $\alpha_s$  are the coefficients for these two quantities. The dimensionless parameter  $B_s$  gives the

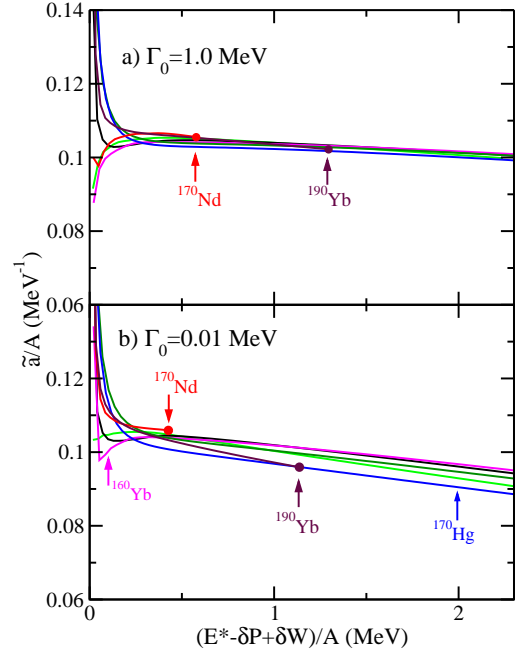


FIG. 14: (Color online) Same as for Fig. 13a, but now the results for  $A \sim 170$  were obtained from the Gamov method with a)  $\Gamma_0 = 1$  MeV and b)  $\Gamma_0 = 0.01$  MeV. Only curves that are distinguishable from the others are labelled.

surface area of the nucleus relative to its spherical value. As all the systems studied are spherical at  $(E^* - \delta P + \delta W)/A = 0.5$  MeV,  $B_s$  was set to unity. The dashed curve in Fig. 17 shows the fit obtained with Eq. 62. The fitted coefficients are  $\alpha_v = 0.078$  MeV $^{-1}$  and  $\alpha_s = 0.146$  MeV $^{-1}$ . For comparison, curves for the level-density parameters from Töke and Światecki ( $\alpha_v = 0.068$  MeV $^{-1}$ ,  $\alpha_s = 0.274$  MeV $^{-1}$ ) [44] and Ignatyuk *et al.* ( $\alpha_v = 0.073$  MeV $^{-1}$ ,  $\alpha_s = 0.095$  MeV $^{-1}$ ) [45] are also displayed. The fitted surface coefficient is intermediate in value between these two other prescriptions, but closer to Ignatyuk *et al.*

Many experimental studies have adopted the excitation-energy dependence of the level density suggested by Ignatyuk *et al.* [2, 45] which includes the washing out of shell effects with increasing temperature. The entropy is expressed in terms of an excitation-energy dependent level-density parameter, i.e.,  $S = 2\sqrt{a(U)U}$  where

$$a(U) = \tilde{a} \left[ 1 + h(U) \frac{\delta W}{U} \right]. \quad (63)$$

The function  $h$ , determining the behavior at low excitation energies, is given by  $h(U) = 1 - \exp(-\gamma U)$ . The parameter  $\gamma$  gives the energy scale over which shell effects are washed out. At high excitation energies where  $h \rightarrow 1$ , the Ignatyuk formalism leads to the expected dependence of Eq. 61. To determine how well Eq. 63 can describe the entropy calculated in this work, asymptotic level-density parameters were determined at each excitation energy

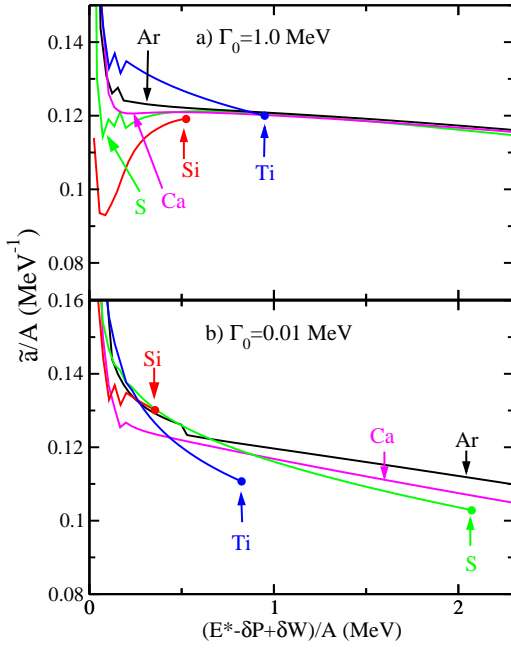


FIG. 15: (Color online) Same as for Fig. 13c, but now the results for  $A=40$  were obtained from the Gamov method with a)  $\Gamma_0=1$  MeV and b)  $\Gamma_0=0.01$  MeV.

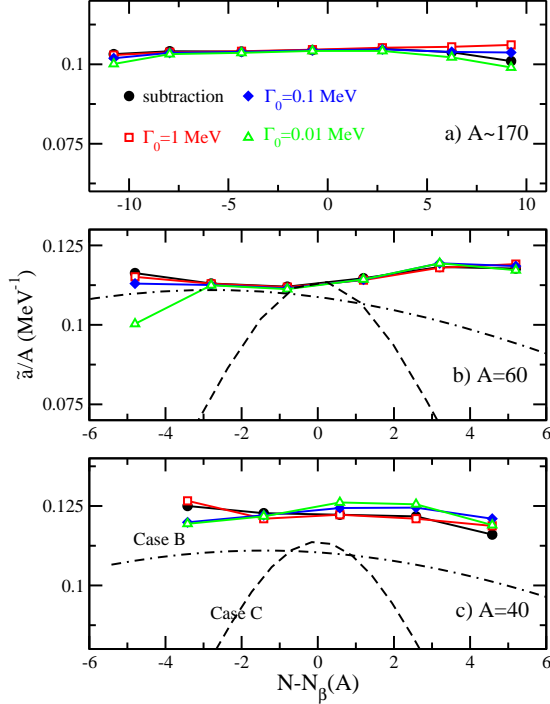


FIG. 16: (Color online) Calculated level-density parameters at  $(E^* - \delta P + \delta W)/A=0.5$  MeV are plotted versus  $N - N_\beta(A)$ , the neutron number separation from the  $\beta$  valley of stability. The data points were obtained with the subtraction and Gamov methods. For the latter, the three indicated value of the cutoff width  $\Gamma_0$  were used. For  $A=40$  and  $60$ , the fitted variation of the level-density parameter (cases B and C) from Ref. [4] are shown by the dot-dashed and dashed curves, respectively.

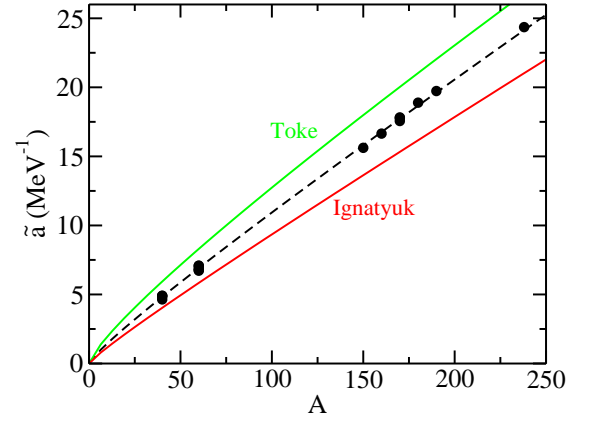


FIG. 17: (Color online) Asymptotic level-density parameter  $\tilde{a}$  as a function of nucleon number  $A$ . The data points are the values determined from the calculations of this work. The dashed curve shows a fit to these data. Curves are also shown for the prescription of Töke and Światecki[44] and Ignatyuk *et al.*[45].

from Eq. 63 and the parameter  $\gamma$  was adjusted to minimize the spread of these deduced  $\tilde{a}$  values at low excitation energies. For the  $A \sim 170$  nuclei,  $\gamma$  was determined by this procedure as  $0.035 \text{ MeV}^{-1}$  and the  $\tilde{a}$  values are plotted in Fig. 18b. These are to be compared to the  $\tilde{a}$  values obtained for  $\gamma=\infty$  in Fig. 18a. The condition  $\gamma=\infty$  corresponds to  $h=0$  and the latter values are the same as deduced from Eq. 61 and plotted in Fig. 13a. The spread in the  $\tilde{a}$  values at low excitation energies observed in Fig. 18a are almost removed in Fig. 18b and thus this indicates that the Ignatyuk formalism describes the fading out of shell effects adequately for this mass region. The deduced value of  $\gamma$  is of similar magnitude to the value  $0.05$  obtained by Ignatyuk *et al.*[45] by fitting neutron resonance data. Schmidt *et al.*[46] have extracted a mass-dependent value of  $\gamma$  and, for  $A=170$ , they find  $\gamma=0.045$ . Again of similar magnitude to the value of this work.

For the lighter mass regions ( $A=40$  and  $60$ ), a similar reduction in the spread of the deduced  $\tilde{a}$  values was not achieved. Thus for these light systems, the description of the level density in the region where shell effects are still important is more complex than this Ignatyuk treatment.

## B. Deformation Dependence

The level density of strongly deformed nuclei is of interest. In the statistical model, the fission decay rate is determined from the level density of the deformed saddle-point configuration. The deformation dependence of the level density is also needed to determine the equilibrium shape distribution of compound nuclei[32]. This distribution can be important in determining the emission rates of  $\alpha$  and heavier fragments[47]. The deformation dependence for  $^{170}\text{Yb}$  at various excitation energies is displayed

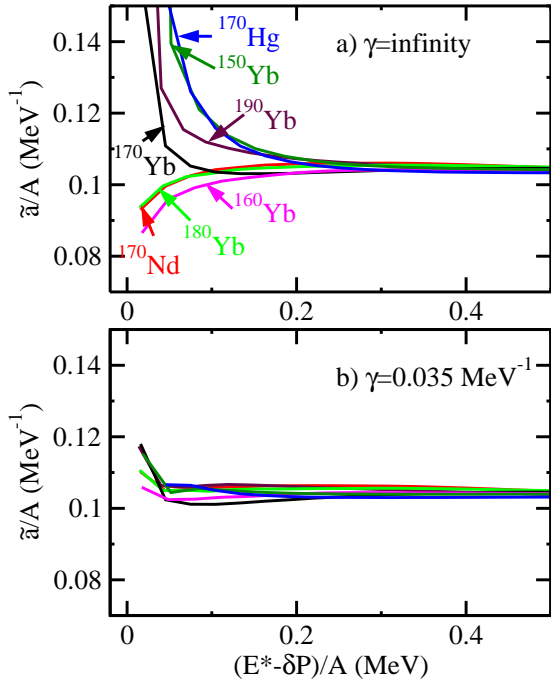


FIG. 18: (Color online) Asymptotic level-density parameters determined for the  $A \sim 170$  systems with Eq. 63. a) The parameter  $\gamma$  was set to infinity. These results are the same as those shown in Fig.13a. b) The value  $\gamma=0.035$  was obtained from minimizing the spread in the curves at low excitation energy.

in Fig. 19. To highlight the deformation dependence, the level densities are normalized to the maximum value for that excitation energy. The results obtained with the subtraction method are shown as the solid curves, while the dashed curves are from the calculation with the Gamov method ( $\Gamma_0=1$  MeV). At the lowest excitation energies, the level density is largest for deformations close to the ground-state value ( $Q=0.875$  for  $^{170}\text{Yb}$ ). For this nucleus at these excitation energies, the continuum is not sampled significantly and the results for the two methods are almost identical. At an intermediate energy ( $\sim 100$  MeV), shell effects have melted and the level density peaks for spherical shapes but the distribution is quite broad. Again, the results are similar for the two methods. However at higher excitation energies where the continuum becomes more important, the results obtained with the two methods are quite different. For the subtraction method (solid curves), the dependence on deformation near sphericity decreases. The curves become broader with increasing excitation energy as expected when the temperature increases. Contrary to this, the dashed curves obtained with the Gamov method becomes narrower. The underlying reason for this behavior can be traced to the variation of the resonance widths with deformation displayed in Fig. 7 and discussed in Sec. IV B. As a spherical system is deformed, then on average, the widths of the resonances increase leading

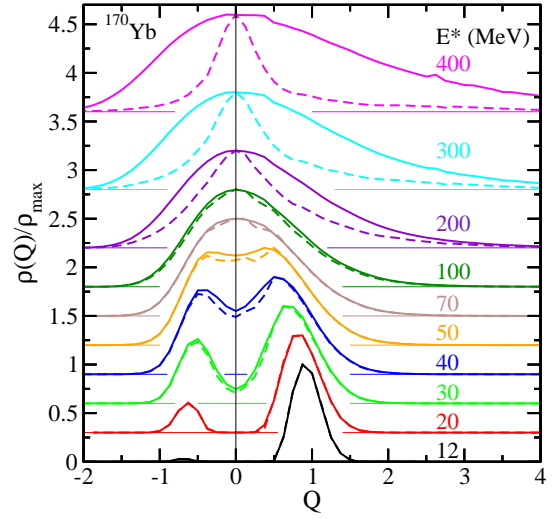


FIG. 19: (Color online) Deformation dependence of the level density calculated for  $^{170}\text{Yb}$  at the indicated excitation energies. The level densities are normalized to the maximum  $\rho_{max}$  for that excitation energy. For clarity the results for each successive excitation energy are shifted up along the  $y$  axis. The thin lines in each case correspond to the shifted  $x$  axis. Results obtained with the subtraction method are shown as the thick-solid curves, while the dashed curve were obtained from the Gamov method with  $\Gamma_0=1$  MeV.

to a decrease in the single-particle level density in the Gamov method. Thus, this behavior leads to a favoring of spherical shapes.

The strong peaking of the level density at sphericity for the Gamov method is quite general. Results are shown in Fig. 20 for  $^{160}\text{Yb}$  and  $^{60}\text{Ni}$  at  $E^*/A = 1.875$  MeV. In both cases, the continuum contributions are significant. Curves are shown for the subtraction method (solid) and for  $\Gamma_0=1$  MeV (dashed) and  $\Gamma_0=0.01$  MeV (dot-dashed). For both nuclei, the level density distributions obtained with the Gamov method are narrower than those from the subtraction method. However, the peaking at sphericity is even stronger for smaller values of the cutoff width  $\Gamma_0$ . Also, the effect is stronger for the heavier system. These dependencies are quite general.

The degree to which the spherical shape is favored in the Gamov method also depends on the  $n-p$  asymmetry. Figure 21 displays the deformation dependence of the level density for three Yb isotopes all at  $E^*/A=1.18$  MeV. The dashed curves, calculated with the Gamov method, indicate that the effect is stronger for the very neutron-rich  $^{190}\text{Yb}$  isotope. Because of the small neutron separation energy for this system, the importance of the positive-energy neutron levels is much greater than for the  $\beta$ -stable  $^{170}\text{Yb}$  system. The proton-rich  $^{150}\text{Yb}$  system shows an even smaller effects than the  $\beta$ -stable nucleus. The most important positive-energy proton levels are below Coulomb the barrier and thus they are all narrow compared to the cutoff width  $\Gamma_0$ . As a general rule, modifications induced by deformation are

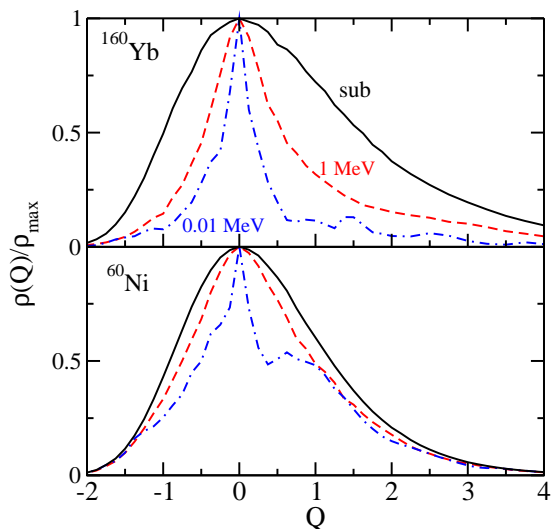


FIG. 20: (Color online) Deformation dependence of the normalized level density as in Fig. 19. Results are shown for  $^{160}\text{Yb}$  ( $E^*=300$  MeV) and  $^{60}\text{Ni}$  ( $E^*=112$  MeV) with the subtraction method (solid curves) and with the Gamov method for  $\Gamma_0=1$  MeV (dashed curves) and 0.01 MeV (dot-dashed curves).

of lesser importance for protons compared to neutrons. Of course for very light nuclei, the Coulomb barrier is smaller and its ability to suppress these deformation effects is reduced.

The deformation dependence from the Gamov method has important consequences for fission. The fission decay width is determined from the ratio of the level densities at the saddle-point and equilibrium configurations. The favoring of spherical nuclei at high excitation energies will lead to a suppression of the fission width and thus an increase in the probability of the competing evaporative decay modes. The total fission cross section will therefore be reduced and, for events that do fission, it will occur later in the decay cascade. Such effects have been observed experimentally. Measurements of pre and postscission multiplicities of evaporated particles in coincidence with fission fragments have shown that these fragments are created with little excitation energy even when the initial CN excitation energy is large[48]. The standard interpretation of these results is in term of dynamical effects[48], but it is clear that if one adopts the Gamov method, then it can explain part, or possibly most, of the experimental observations. The magnitude of the predicted effect will depend on the value of  $\Gamma_0$ .

Fission is most important for the heavier systems and thus it is of interest to examine the deformation dependence determined for  $^{238}\text{U}$ . This is shown in Fig. 22 for three excitation energies. For the lowest value ( $E^*=16$  MeV), the level density is again largest for deformations around the ground-state value. There is again no difference between the subtraction (solid curve) and Gamov (dashed curve) methods. (The curves are indis-

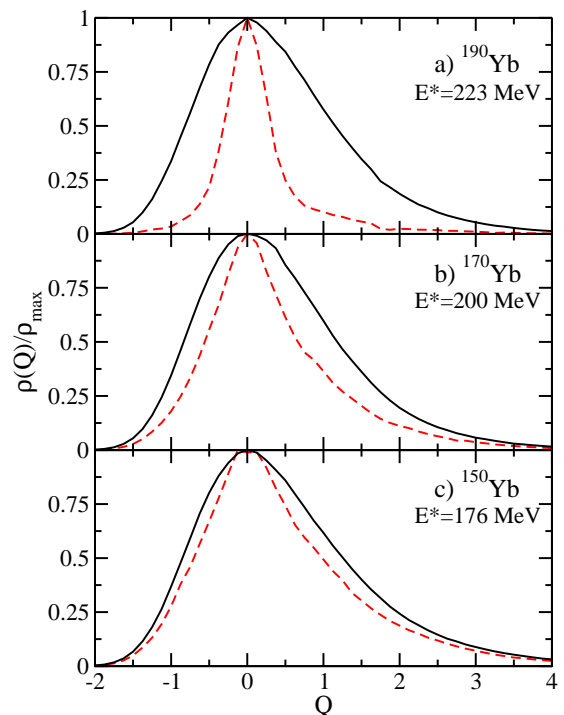


FIG. 21: (Color online) Deformation dependence of the normalized level density for three Yb isotopes at the indicated excitation energies. Solid and dashed curves were obtained with the subtraction and Gamov ( $\Gamma_0=1$  MeV) methods, respectively.

tinguishable). At  $E^*=140$  MeV shell effects have melted and, in both methods, the level density is largest for spherical systems. Only a small difference between the two methods is observed. Again at the highest excitation energy ( $E^*=560$  MeV), the two methods give very different results. The Gamov method is strongly peaked at sphericity. In contrast now, the results with the subtraction method show this nucleus is unstable with respect to prolate deformations, i.e., the level density increases with increasing  $Q$ . This is basically a fission instability, however to fully treat fission one should include more shape degrees of freedom. If the level-density parameter is deformation dependent as in Eq. 62, then the fission barrier is temperature dependent[49]. The result obtained with the subtraction method therefore represents the situation where the temperature-dependent fission barrier has vanished. In terms of level density, there is no saddle-point, i.e., a configuration of low level density which represents a bottleneck through which the system must pass in order to fission. Therefore, fission stability can be quite different for the two methods of treating the continuum.

As the deformation-dependence of the level-density parameter plays an important role in fission, the applicability of Eq. 62 was investigated for the subtraction method. (It is clearly not applicable for the Gamov method). For a given excitation energy and deformation, the asymp-

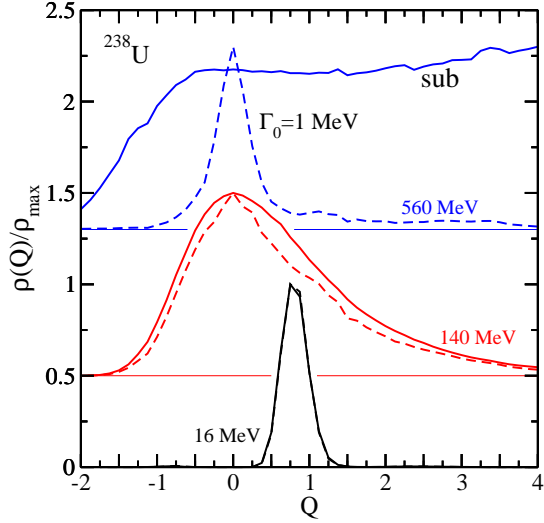


FIG. 22: (Color online) Deformation dependence of the normalized level density for  $^{238}\text{U}$  as in Fig. 19.

otic level-density parameter was determined as

$$S = 2\sqrt{\tilde{a}(E^* - \delta P + \delta W - V_{def}(Q))} \quad (64)$$

assuming shell and pairing effects are washed out. This differs from Eq. 61 in that now the liquid-drop deformation energy has also been subtracted from the excitation energy. Results obtained for  $^{150}\text{Yb}$  are displayed in Fig. 23 as the data points for various values of  $E_{th} = E^* - \delta P + \delta W - V_{def}(Q)$ , the asymptotic thermal excitation energy. The extracted values are plotted against  $B_s$ , the relative surface area ( $B_s=1$  is sphericity). Except for the lowest value of  $E_{th}$  where shell oscillations are still present, they increase almost linearly with  $B_s$ . The solid curves display linear fits to the extracted values and, from the fitted slopes, the surface coefficient  $\alpha_s$  (Eq. 62) can be determined. Ignoring  $E_{th}=70$  MeV, the slopes, and thus the  $\alpha_s$  coefficients, are almost independent of excitation energy. The  $\alpha_s$  coefficients obtained from all calculated  $A \sim 170$  nuclei are plotted in Fig. 24. Apart from the lowest excitation energies where shell effects are still important, all the  $\alpha_s$  coefficients are similar, almost independent of excitation energy and  $n-p$  asymmetry. The values of  $\alpha_s$  determined by this procedure are quite similar to the value obtained from fitting the  $A$  dependence of  $\tilde{a}$  in Sec. VII A. This value is indicated by the dotted line in Fig. 24. Clearly Eq. 62 provides a reasonably consistent description of the  $A$  and deformation dependencies of the level-density parameter for the subtraction method. The small difference between the extracted values of  $\alpha_s$  from the two procedures may be due to the fact that curvature and higher-order corrections to the level-density parameter[44] have been ignored. Thus, these must be small (at least for the deformations considered) in order to get such good agreement from the two procedures.

One final note,  $\alpha_s$  depends very much on details of

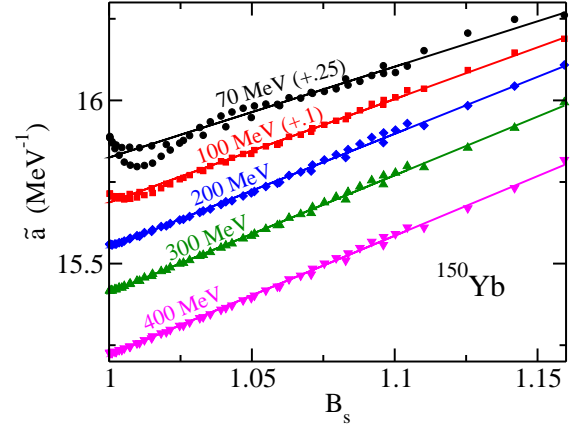


FIG. 23: (Color online) Asymptotic level-density parameters deduced for deformed  $^{150}\text{Yb}$  nuclei (oblate and prolate shapes) as a function of the relative surface area  $B_s$ . Results are shown for the indicated thermal excitation energies. For clarity, results at some excitation energies have been shifted up along the  $y$  axis by the indicated amounts.

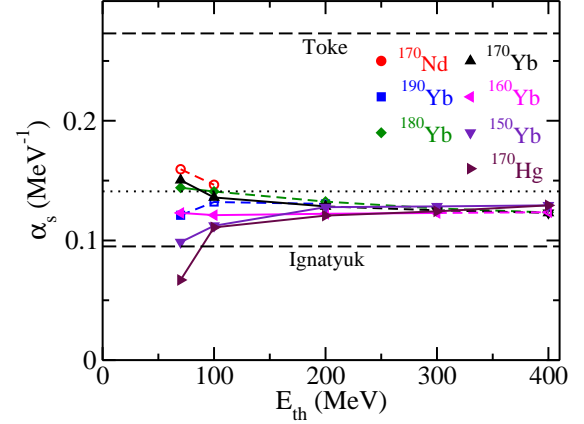


FIG. 24: (Color online) Surface coefficient of the level-density parameter obtained for the  $A \sim 170$  systems as a function of excitation energy. The dotted line indicates the value obtained from the fit in Fig. 17. Other values of the surface coefficient, from the prescriptions of Töke and Świątecki[44] and Ignatyuk *et al.*[45], are also indicated.

how the mean-field potential changes with deformation. In Sec. IV A, the diffuseness parameter  $d$  of the nuclear potential was made angle dependent (Eq. 26) so that the diffuseness perpendicular to the nuclear surface is constant. The parameter  $d$  is actually the diffuseness along the radial direction. If instead  $d$  is set to be constant as in many studies, then the extracted  $\alpha_s$  values were found to be negative! In this case, the mean diffuseness perpendicular to the nuclear surface decreases with deformation. As the level-density parameter is quite sensitive to the diffuseness, this leads to the calculated reduction of the level-density parameter with deformation. Thus for large deformations, it is important to make  $d$  angle dependent.

### VIII. DISCUSSION

In the preceding section, it was shown that the two methods for calculating the contribution from the positive-energy single-particles levels give similar results, apart from the deformation dependence. The difference between the two methods are the inclusion of both the negative background and the wide resonances in the subtraction method. These two contributions have opposite effects on the level density, and thus it seems they partially cancel each other. Also for heavy systems with large Coulomb barriers, the low, positive-energy proton states are all narrow resonances and thus give almost identical results for the two methods. Thus the proton-rich side of the chart of nuclides is less sensitive than the neutron-rich side to the continuum, at least for the heavier systems.

If the Gamov method is considered preferable, then consideration must be given to the value of  $\Gamma_0$ . Possibly  $\Gamma_0$  is related to the CN lifetime, i.e., only Gamov levels of lifetime greater than the CN should be considered. As the CN lifetime decreases with excitation energy, then  $\Gamma_0$  should increase. An increasing value of  $\Gamma_0$  with excitation energy would lead to a reduction in the predicted strong peaking of the level density at sphericity. Another possibility is that  $\Gamma_0$  should be related to the average spreading width of levels near the Fermi surface. This would lead to a much smaller excitation-energy dependence of  $\Gamma_0$ .

It is important to remember that the results of this work relate to how the treatment of positive-energy single-particle levels affects the level density in the independent-particle model. Apart from pairing, the calculations did not include any other many-body effects. Also they did not allow for selfconsistency between the assumed nuclear potential and predicted density distributions of the nucleons. These effects may lead to deviations from the predicted behavior. In fact, experimentally it is known that the level density for hot Yb nuclei cannot be described by a backshifted Fermi-gas expression, but an important excitation-energy dependence of the level-density parameter is needed[1]. The latter is consistent with the variation of the frequency-dependent effective nucleon mass with temperature[50].

Some of the effects ignored in this work may influence the  $n$ - $p$  asymmetry dependence. For example, if the diffuseness parameter of the nuclear potential increases for nuclei close to the drip lines, then this will enhance the level-density parameter for these systems. Also differences between the neutron and proton effective masses and their dependence on asymmetry may also be important.

Al-Quraishi *et al.*[4] had suggested that a restriction of the positive-energy states to narrow resonances, as in the Gamov method, would lead to an important  $n$ - $p$  asymmetry dependence of the level-density parameter. They fit the density of known levels for  $20 \leq A \leq 70$  with the

form

$$a_C = a_1 A \exp \left\{ a_2 [Z - Z_\beta(A)]^2 \right\} \quad (65)$$

where  $Z_\beta(A)$  is the proton number of the  $\beta$ -stable nucleus of nucleon number  $A$  and  $a_1$  and  $a_2$  are the fit parameters. This is called case C in Ref. [4]. The dashed curves in Figs. 16b and 16c show  $a_C$  for  $A=60$  and 40, respectively. If this strong  $n$ - $p$  asymmetry dependence is real, the calculations of this work suggest it cannot be explained by the treatment of the continuum as assumed in the justification of Eq. 65. Al-Quraishi *et al.* also considered another fit (case B) based on isospin considerations:

$$a_B = a_3 A \exp \left[ a_4 (N - Z)^2 \right] \quad (66)$$

where now  $a_3$  and  $a_4$  are the fit parameters. The dot-dashed curves in Figs. 16b and 16c show the resulting values of  $a_B$ . In this case, the  $n$ - $p$  asymmetry dependence is not as strong as in case C, but still stronger than our calculations for  $A=60$ . The large difference between cases B and C suggests the fits do not constrain the level-density parameter for very neutron and proton-rich nuclei. In Ref. [1], no significant asymmetry dependence of the level-density parameter was observed for  $^{152}\text{Yb}$  and  $^{160}\text{Yb}$  CN with excitation energy greater than 100 MeV. This is consistent with the dependence calculated with both methods of this work (see Figs. 16a).

It is also important to note again that the small  $n$ - $p$  asymmetry dependence observed in these calculations is only true for  $T < E_{cost}^{\min}$ . Extending the calculations above  $T = E_{cost}^{\min}$  leads to a much larger dependence, although this region is not relevant to the statistical model. In Ref. [18] it was noted that for calculations where the number of single-particle levels is finite, such as in the Gamov method, then there is a maximum excitation energy of the CN. The level density as a function of excitation energy must peak and then approach zero at this maximum excitation energy. The peak value of the level density corresponds to  $T=\infty$  and higher excitation energies have negative temperatures. The details of this behavior would be very dependent on the  $n$ - $p$  asymmetry. Although a negative temperature may be appropriate for the CN, it is certainly not meaningful for the gas. Thus our model of CN in equilibrium with the surrounding gas breaks down. However, it is not clear that this is of any relevance for the statistical model.

### IX. CONCLUSIONS

The effects of continuum positive-energy neutron and proton levels on the nuclear level density has been investigated. The use of the independent-particle model allowed for a broad survey of how these continuum corrections modify the level density over the entire chart of nuclides. Two methods for calculating the contributions of these positive-energy levels were investigated. In the

subtraction method, the single-particle level density is determined from the scattering phase shifts. The resulting single-particle level density has contributions from narrow and wide resonances and a negative background. In the Gamov method, the single-particle level density is calculated from the Gamov states and only the contributions from the narrow resonances are considered. From the bound states and these two prescriptions for the positive-energy states, the entropy and level density are calculated as a function of temperature and excitation energy. These calculations ignored all many-body effects apart from the pairing interaction. At large excitation energies where shell effects melt, the level density followed a backshifted Fermi-gas expression. Also, the deduced level-density parameters were quite similar for the two methods. They depend on  $A$  with very little dependence on the  $n$ - $p$  asymmetry of the nucleus. The biggest asymmetry dependence was for the very exotic systems near the drip lines where a small reduction in the level-density parameter was sometimes found. For the heavier systems, the prescription of Ignatyuk *et al.*[45] accounted for the variation in level density at low excitation energies where shell effects are still important.

The largest differences arising from the use of the two methods was the predicted deformation dependence of the level density. At high excitation energies, the Gamov method predicted the level density peaked strongly for spherical systems whereas in the subtraction method the deformation dependence was rather flat near sphericity. This suppression in the relative level densities of deformed to spherical systems in the Gamov method would lead to a reduction in the predicted fission width and may help explain the large prescission light-particle multiplicities observed in fission reactions[48].

### Acknowledgments

We wish to acknowledge many informative discussions with Prof. Ron Lovett and Prof. Willem Dickhoff. This work was supported by the Director, Office of High Energy and Nuclear Physics, Nuclear Physics Division of the U.S. Department of Energy under contract number DE-FG02-87ER-40316.

- 
- [1] R. J. Charity, L. G. Sobotka, J. F. Dempsey, M. Devlin, S. Komarov, D. G. Sarantites, A. L. Caraley, R. T. DeSouza, W. Loveland, D. Peterson, et al., *Phys. Rev. C* **67**, 044611 (2003).
- [2] A. V. Ignatyuk, K. K. Istekov, and G. N. Smirenkin, *Sov. J. Nucl. Phys.* **29**, 450 (1979).
- [3] Z. Y. Ma and J. Wambach, *Nucl. Phys.* **A402**, 275 (1983).
- [4] S. I. Al-Quraishi, S. M. Grimes, T. N. Massey, and D. A. Resler, *Phys. Rev. C* **63**, 065803 (2001).
- [5] P. J. Siemens and A. S. Jensen, *Elements of Nuclei* (Addison-Wesley, Redwood City, 1987).
- [6] A. Bohr and B. R. Mottelson, *Nuclear Structure*, vol. I (Benjamin, New York, 1975).
- [7] H. A. Bethe, *Phys. Rev.* **50**, 332 (1936).
- [8] K. J. L. Couter and W. D. Lang, *Nucl. Phys.* **13**, 32 (1959).
- [9] W. A. Fowler, C. A. Engelbrecht, and S. E. Woosley, *Ap. J.* **226**, 984 (1978).
- [10] E. Beth and G. E. Uhlenbeck, *Physica* **4**, 915 (1937).
- [11] D. R. Dean and U. Mosel, *Z. Phys. A* **322**, 647 (1985).
- [12] S. Shlomo, V. M. Kolomietz, and H. Dejbakhsh, *Phys. Rev. C* **55**, 1972 (1997).
- [13] R. G. Newton, *Scattering Theory of Waves and Particles* (Dover, New York, 2002).
- [14] T. Y. Tsang and T. A. Osborne, *Nucl. Phys.* **A247**, 43 (1975).
- [15] T. A. Osborn and T. Y. Tsang, *Ann. of Phys. (NY)* **101**, 119 (1976).
- [16] T. A. Osborn and D. Bollé, *J. Math. Phys.* **18**, 432 (1977).
- [17] H. A. Weidenmüller, *Phys. Lett.* **10**, 331 (1964).
- [18] M. G. Mustafa, M. Blann, A. V. Ignatyuk, and S. M. Grimes, *Phys. Rev. C* **45**, 1078 (1992).
- [19] A. Böhm, *Quantum Mechanics* (Springer-Verlag, New York, 1979).
- [20] G. Gamov, *Z. Phys.* **51**, 204 (1928).
- [21] R. W. Hasse and W. D. Myers, *Geometric Relationships of Macroscopic Nuclear Physics* (Springer-Verlag, Berlin, 1988).
- [22] H. Esbensen and C. N. Davids, *Phys. Rev. C* **63**, 014315 (2000).
- [23] J. Binney and S. Tremaine, *Galactic Dynamics* (Princeton University Press, Princeton, NJ, 1987).
- [24] S. Chandrasekhar, *Ellipsoidal Figures of Equilibrium* (Dover, New York, 1987).
- [25] J. Dudek, Z. Szymański, T. Werner, A. Faessler, and C. Lima, *Phys. Rev. C* **26**, 1712 (1982).
- [26] B. R. Johnson, *J. Chem. Phys.* **69**, 4678 (1978).
- [27] B. R. Johnson, *J. Computational Phys.* **13**, 445 (1973).
- [28] D. E. Manolopoulos, *J. Chem. Phys.* **85**, 6425 (1986).
- [29] F. Mrugała and D. Secrest, *J. Chem. Phys.* **78**, 5954 (1983).
- [30] N. Sandulescu, O. Civitarese, R. J. Liotta, and T. Vertse, *Phys. Rev. C* **55**, 1250 (1996).
- [31] M. Santo and S. Yamasaki, *Prog. Theor. Phys.* **29**, 397 (1963).
- [32] L. G. Moretto, *Nucl. Phys.* **A185**, 145 (1971).
- [33] A. S. Jensen and J. Damgaard, *Nucl. Phys.* **A203**, 578 (1973).
- [34] V. M. Strutinsky, *Nucl. Phys.* **A95**, 420 (1967).
- [35] V. M. Strutinsky, *Sov. J. Nucl. Phys.* **3**, 449 (1969).
- [36] M. Brack and H. C. Pauli, *Nucl. Phys.* **A207**, 401 (1973).
- [37] T. Vertse, A. T. Kruppa, R. J. Liotta, W. Nazarewicz, N. Sandulescu, and T. R. Werner, *Phys. Rev. C* **57**, 3089 (1998).
- [38] T. Vertse, A. T. Kruppa, and W. Nazarewicz, *Phys. Rev. C* **61**, 064317 (2000).

- [39] W. D. Myers and W. J. Swiatecki, Nucl. Phys. **81**, 1 (1966).
- [40] W. D. Myers and W. J. Swiatecki, Ark. Fys. **36**, 343 (1967).
- [41] L. G. Moretto, Nucl. Phys. **A185**, 145 (1972).
- [42] J. R. Huizenga and L. G. Moretto, Ann. Revs. Nucl. Sci. **22**, 427 (1972).
- [43] P. Bonche, S. Levit, and D. Vautherin, Nucl. Phys. **A427**, 278 (1984).
- [44] J. Töke and W. Światecki, Nucl. Phys. **A372**, 141 (1981).
- [45] V. Ignatyuk, N. Smirenkin, and A. Tishin, Sov. J. Nucl. Phys. **21**, 255 (1975).
- [46] K.-H. Schmidt, D. Delagrange, J. P. Dufour, N. Căjan, and A. Fleury, Z. Phys. A **308**, 215 (1982).
- [47] R. J. Charity, Phys. Rev. C **61**, 054614 (2000).
- [48] D. Hilscher and H. Rossner, Ann. Phys. (Paris) **17**, 471 (1992).
- [49] R. J. Charity, Phys. Rev. C **53**, 512 (1996).
- [50] P. F. Bortignon and C. H. Dasso, Phys. Lett. B **189**, 381 (1987).